Research Article

Luiz Manuel Braga da Costa Campos, Manuel José dos Santos Silva*, and João Manuel Gonçalves de Sousa Oliveira

On the effects of rough ground and atmospheric absorption on aircraft noise

https://doi.org/10.1515/noise-2022-0003
Received Jan 24, 2021; accepted Jan 22, 2022

Abstract: The noise received from an aircraft is modified by atmospheric attenuation and reflections from the ground. The interference of direct and reflected waves is simplest for a flat ground, whereas multiple reflections can occur for rough ground or mountainous surroundings. The ground characteristics, like reflection and absorption factors or impedance, also affect the received sound. All these effects have to be considered with respect to the path of the aircraft. Most of the literature about ground effects on aircraft noise considers a point source over a flat ground, using the method of images, that does not extend readily to rough ground. The effect of rough ground on aircraft noise can be modelled by: (i) identification of reflection points (there may be several points); (ii) use of a complex reflection coefficient (with amplitude and phase changes) at each reflection point; (iii) adding all reflected waves within line-of-sight of the receiver, that is not blocked by terrain (there is no blockage for a flat ground).

Keywords: direct signal, reflected signal, ground profile, atmospheric attenuation, multipath factor

1 Introduction

The aircraft noise is a significant environmental issue for residents near airports, and has been a major topic in the literature from the last century [1] to the present [2]. The aircraft noise can lead to: (i) curfews, limiting the operating hours of airports, such as forbidding night flights; (ii) local noise limits, which may be more restrictive than the ICAO certification rules, and thus limit the take-off weight and hence payload-range with an adverse effect on operating economics. The helicopter noise is the main limitation in their use over urban and populated areas, affecting medical emergencies, law enforcement, city centre business travel and other services. The emerging market for UAM (Urban Air Mobility) using e-VTOL (electric powered Vertical Take-Off and Landing) aircraft is subject to noise limitations similar to helicopters. The decreasing tolerance of local communities to aircraft and helicopter noise stands in contrast to the long term growth of long range and local air transport.

The two main aspects of aircraft noise are: (i) atmospheric propagation [3–11] including the effects of stratification leading to not only non-uniform sound speed, but also convection and refraction by wind and turbulence; (ii) ground effects considered in most of the literature [12–20] by a source and its image on a flat impedance ground, including the lateral wave. Ground effects on sound can be more complex: (i) the presence of obstacles like buildings and other constructions leads to corner reflections [21, 22] with three reflected waves instead of one form flat ground, in addition to the direct wave from the sound source; (ii) the current methods of calculation of noise contours around airports [23, 24] are based on models of sound propagation over flat ground [25–28], and do not account for the variable elevations of rough ground that may surround the airport. The main aim of the present paper is to consider (a) sound reflection over a rough ground using (b) a method of wave reflection distinct from the image source method, as shown in the Figure 1. These two differences from the usual approach in the literature are discussed briefly next and in more detail in the conclusion.

The effect of a flat ground on the sound emitted by real sound source can be represented by a virtual image source emitting a virtual wave to the observer. The sum of the direct and virtual waves satisfies the boundary condition on the ground. Instead of a virtual source, and closer to physi-

***Corresponding Author: Manuel José dos Santos Silva:** CCTAE, IDMEC, LAETA, Instituto Superior Técnico, Universidade de Lisboa, Av. Rovisco Pais 1, 1049-001, Lisboa, Portugal; Email: manuel.jose.dos.santos.silva@tecnico.ulisboa.pt
Luiz Manuel Braga da Costa Campos: CCTAE, IDMEC, LAETA, Instituto Superior Técnico, Universidade de Lisboa, Av. Rovisco Pais 1, 1049-001, Lisboa, Portugal; Email: luis.campos@tecnico.ulisboa.pt
João Manuel Gonçalves de Sousa Oliveira: CCTAE, IDMEC, LAETA, Instituto Superior Técnico, Universidade de Lisboa, Av. Rovisco Pais 1, 1049-001, Lisboa, Portugal; Email: joliveira@tecnico.ulisboa.pt

cal reality, the ground effect is equivalent to adding to the direct wave from the source to the observer another wave reflected from the ground. This method is simple and quite general since the reflection coefficient on the ground can be complex, introducing both amplitude and phase changes in the reflected wave. This method has been applied to sound reflection in a corner [21] involving three reflected waves. An alternative would have been to use three images [22] in the corner. The method of images does not extend easily to reflection by a rough ground, since it could require several images and the determination of their strength and location. The method of reflection extends readily from flat to rough ground by: (i) determining geometrically all reflection points; (ii) applying the complex reflection coefficient, including amplitude and phase, at each point; (iii) adding all waves that can be radiated towards the observer, that are not blocked by the terrain. The latter effect of wave blockage by terrain elevation is not present for flat ground.

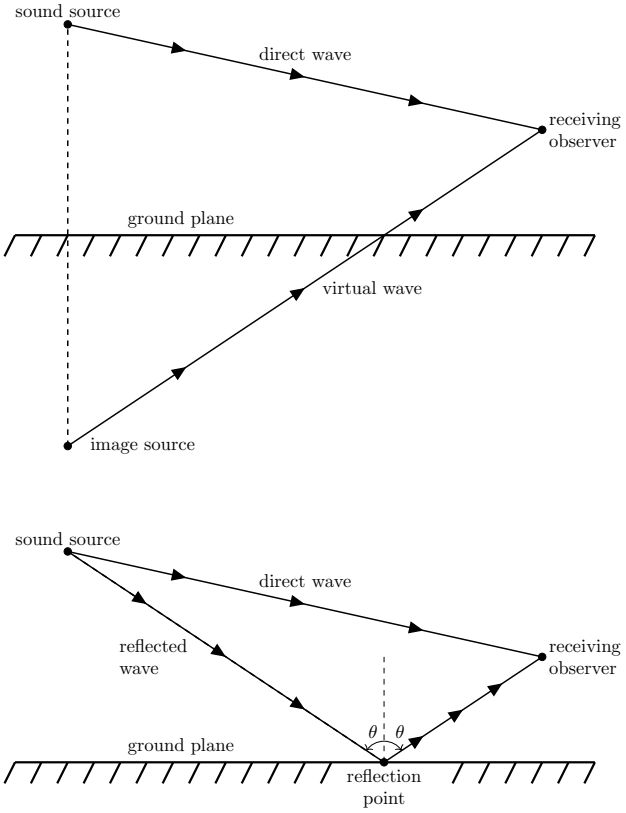

Figure 1: Comparison of (I) the method of image (top) and (II) the method of reflection (bottom) for a point sound source above a plane. In both cases, there is a direct wave from the sound source to the receiving observer, as in free space. The ground effect is represented: (I) in the image method by adding a virtual wave from the image source to the receiving observer so as to satisfy the acoustic boundary condition on the ground plane; (II) in the reflection method by adding a reflected wave making an equal angle θ of incidence and reflection relative to the normal at the reflection point, with a complex reflection coefficient accounting for amplitude and phase changes.

In addition to sound reflection from rough ground, the effect of atmospheric absorption is also considered. Concerning ground reflection, it is convenient to start with the simplest cases for reference as more effects are added. In the case of a point sound source over flat ground, there is: (i) a direct wave from the source to the observer; (ii) a wave with an intermediate reflection on the ground. Since the original and reflected waves are travelling in the same medium and consequently the frequency of both waves is the same, the resultant sound pressure level depends on the phase difference between the two sound waves, and consequently the worst-case scenario happens when they are in-phase, duplicating the total amplitude and increasing $20\log_{10} 2 = 6\,\text{dB}$ for the power. If the waves are out-of-phase, there is less amplification and they can even cancel each other out when they have exactly opposite phases. Furthermore, if the ground does not perfectly reflect the wave, then the existence of a reflected wave reduces the total amplitude perceived by the observer. The present paper studies, in two-dimensional cases, the interference between the direct and reflected waves, resulting on the amplification, attenuation or cancellation. The interference depends on the frequency and positions of the source and receiver addressing specifically the effects on the aircraft noise that result from the sound reflection on irregular ground and atmospheric absorption.

The baseline model I, as sketched in the Figure 2, uses a single reflection point over flat ground and relies on the following assumptions: (i) isotropic, point source of sound emitting spherical waves (valid if the distance of observer is large relative to the helicopter or aircraft size); (ii) static source (neglects Doppler effects for aircraft speed small relative to sound speed); (iii) flat, horizontal ground (excludes mountainous ground and obstacles, hence there are no multipath effects or wide area or multiple scattering);

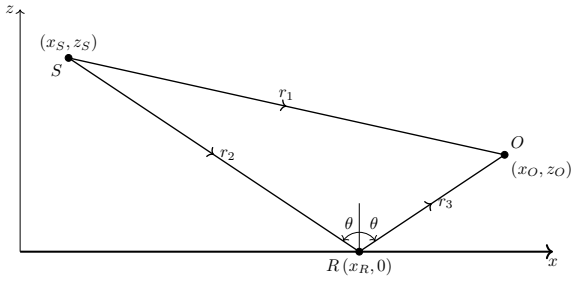

Figure 2: Direct and reflected sound paths for source and observer at arbitrary positions over a flat ground.

(iv) homogeneous atmosphere (neglects density and temperature variations, or sound speed stratification, hence no refraction effects); (v) atmosphere at rest (no wind or mean flow convection or turbulence effects on sound); (vi) uniform ground impedance (same ground composition everywhere all the time, excluding different soils, humidity, changes during the day, etc.).

This simplest baseline model I serves as a reference for two extensions that relax some of its restrictions to include: (i) non-flat ground considering multiple paths in the model II; (ii) atmospheric absorption in the case of uneven ground extending the model II to the model III. The application of all three models depends on the calculation of reflection points, which is done for: (i) reflection from a flat ground, applicable to the models I and III; (ii) reflection from a two-dimensional slice of ground, applicable to the model II. For each of these models, formulas for the SPL (sound pressure level) variation and the phase shift of acoustic pressure are presented.

As examples of the applications from this set of three models, two cases are considered: (i) flat impedance ground using the model I; (ii) rigid undulating ground using the model II. The general theory for the three models and two applications substantiate some conclusions.

2 Baseline model I of reflection by flat ground

The baseline model I relies on the assumption indicated in the introduction. The Figure 2 shows the source-observer coordinate system: (i) the x-axis is horizontal and the z-axis is vertical in the vertical plane passing through the source S and observer O; (ii) the y-axis forms a right-handed triad, and the origin is any point on the intersection of the vertical plane with the ground. For definiteness, the origin may be taken on the ground, for instance in the vertical through the observer, in which case $x_O = 0$ according to the Figure 2. The section 6 will prove that only the horizontal distance between the observer and source matters and not the explicit values of both horizontal coordinates.

The problem of several paths of propagation and interferences can be applied to all waves, in this paper particularly to acoustic waves. The Figure 2 illustrates the two-dimensional case of propagation of acoustic waves, where it is shown that the observer (or monitoring device) receives two signals: (i) one direct signal from the source; (ii) one signal reflected from the ground. Following a purely geometric methodology, it is necessary to determine the position of the reflection point to calculate the length of all the ray paths, making use of the Snell's law of specular reflection: the angle between the normal to the surface and incident wave must be equal to the angle between the same normal and reflected wave. Finally, knowing the value of the reflection coefficient at the reflection point, the total received signal can be specified and then it can be normalized with the direct wave, specifying the modification factors, generally complex numbers, due to multipath effects.

Using the vertical plane through the source and observer, i.e. the line-of-sight plane, consider the two-dimensional problem of wave propagation from a source S to an observer O near a horizontal ground $z = 0$ taken as an axis of a Cartesian reference with the origin at some point on the ground and in such a way that the coordinates of the observer are (x_O, z_O) and the coordinates of the source are (x_S, z_S). The direct received acoustic pressure is

$$p_0 = \frac{\mathrm{e}^{\mathrm{i}kr_1}}{r_1} \tag{1}$$

where a complex constant amplitude and a frequency factor $\exp(\mathrm{i}\omega t)$ are omitted, and r_1 is the distance from the observer to the source:

$$r_1 \equiv \left|(x_O - x_S)^2 + (z_O - z_S)^2\right|^{1/2}. \tag{2}$$

The Eq. (1) is an harmonic solution of the linearised wave equation assuming that the pressure perturbation is radial and propagates spherically outward from the source. The wave equation can be deduced assuming that the sound is a weak motion of an inviscid fluid since the viscosity for the sound field in air at the most audible frequencies is negligible, neglecting thermal conduction and noting that the air before perturbed by acoustic waves is at rest. Because the acoustic waves induce small perturbations in the medium, the wave equation can be linearised. The physical meaning can be given by the real part of (1).

The line-of-sight reflection occurs at the reflection point $R \equiv (x_R, 0)$, such that the angles of incidence and reflection θ are the same,

$$\frac{x_O - x_R}{z_O} = \tan\theta = \frac{x_R - x_S}{z_S}. \tag{3}$$

This can be solved for x_R,

$$x_R = \frac{x_O z_S + x_S z_O}{z_O + z_S}, \tag{4}$$

to specify the position of the point-of-reflection. The sound field reflected in line-of-sight,

$$p_r = \mathcal{R}\frac{\mathrm{e}^{\mathrm{i}k(r_2+r_3)}}{r_2 + r_3}, \tag{5}$$

consists of: (i) a spherical wave travelling from the sound source to the reflection point at a distance

$$r_2 \equiv \left|(x_S - x_R)^2 + z_S^2\right|^{1/2} \tag{6}$$

and from the reflection point to the observer at a distance

$$r_3 \equiv \left|(x_O - x_R)^2 + z_O^2\right|^{1/2}; \tag{7}$$

(ii) a complex reflection coefficient of the ground, which can have a modulus $|\mathcal{R}| \leq 1$ and a phase angle $\arg(\mathcal{R})$, and depends on ground properties. Again, (5) is an harmonic solution of the linearised wave equation where the physical solution can be given by its real part. This solution is modified by the complex reflection factor $\mathcal{R}$ at the reflection point. The lateral wave resulting from the reflection of a spherical wave with a flat ground [12, 15, 16, 18, 20] is neglected, since it is a surface wave that decays away from the ground.

As the presence of an acoustic wave is a small perturbation, the product of two perturbations are neglected and the laws describing the propagation are linear. Consequently, the interaction between the reflected and direct waves is negligible and the total acoustic field is a result of superposition method, summing the results of both waves. Hence, the total acoustic pressure perturbation,

$$p_I = p_0 + p_r = \frac{e^{ikr_1}}{r_1} + \mathcal{R}\frac{e^{ik(r_2+r_3)}}{r_2+r_3}, \tag{8}$$

is the sum of the direct (1) and reflected (5) acoustic pressure perturbations.

The total signal (8) normalized to the direct signal (1) specifies the amplitude and phase changes due to the presence of a reflected wave and is called the multipath factor. Since it is defined as the ratio between two complex acoustic pressure perturbations, assuming that they are harmonic solutions of the linearised outward spherical wave equation, centred from the source, the multipath factor is also generally complex; the modulus and phase of the multipath factor specify respectively the amplitude and phase changes of the received signal that can be analysed separately. The SPL change in the Eq. (10b) and the phase change in the Eq. (11b) of the acoustic pressure perturbation are valid for arbitrary reflection factor $\mathcal{R}$, which may involve an amplitude $|\mathcal{R}|$ and a phase $\arg(\mathcal{R})$. The effect of the ground reflection on the acoustic energy of the free acoustic field corresponds to the complex magnitude of the multipath factor,

$$E_I = \frac{|p_I|^2}{|p_0|^2} = \left|1 + \frac{p_r}{p_0}\right|^2, \tag{9}$$

and in the present case is

$$E_I = \left|1 + \frac{r_1}{r_2+r_3}\mathcal{R}e^{ik(r_2+r_3-r_1)}\right|^2. \tag{10a}$$

This corresponds to a change in SPL (Sound Pressure Level) for power in a decibel (dB) scale

$$A_I = 10\log E_I = 10\log\left\{1 + \left(\frac{r_1}{r_2+r_3}\right)^2|\mathcal{R}|^2 + \frac{2r_1|\mathcal{R}|}{r_2+r_3}\cos\left[k(r_2+r_3-r_1)+\arg(\mathcal{R})\right]\right\}. \tag{10b}$$

The amplitude change depends on all the three ray distances and on the reflection coefficient (not only its modulus, but also its phase). It is also dependent on the frequency of the acoustic waves. In the particular case when the receiver is near the ground, that is when the points O and R nearly coincide, the distance travelled by the reflected wave is the same as the distance travelled by the direct wave, $r_1 = r_2 + r_3$. In that case, $p_r = \mathcal{R}p_0$ or equivalently $p_I = (1+\mathcal{R})p_0$. The reflected wave changes the acoustic pressure perturbation by the factor $1 + \mathcal{R}$ and changes the SPL in decibels by $10\log\left\{1 + |\mathcal{R}|^2 + 2|\mathcal{R}|\cos\left[\arg(\mathcal{R})\right]\right\}$. If both waves travel the same distance, the multipath factor does not depend on the frequency. If the phase of the wave does not change when it impinges on the ground, $\arg(\mathcal{R}) = 0$, usually set for an acoustically hard boundary, the change of SPL reduces to $20\log\{1 + |\mathcal{R}|\}$, and moreover if the boundary totally reflects the wave, $|\mathcal{R}| = 1$, the total acoustic pressure perturbation is doubled leading to the increase of 6.02 dB. Indeed, in that particularly case, when the ground does not change neither the phase wave nor the modulus of the wave and the distance travelled by both waves is the same, the observer receives two waves of the same frequency, same amplitude and in the same phase. The phase of the acoustic pressure perturbation has a variation

$$\Phi_I = \arg(p_I) - \arg(p_0) = \arg\left(\frac{p_I}{p_0}\right) = \operatorname{arccot}\left[\frac{\operatorname{Re}(p_I/p_0)}{\operatorname{Im}(p_I/p_0)}\right] \tag{11a}$$

and is given in the case (10b) by

$$\Phi_I = \operatorname{arccot}\left\{\cot\left[k(r_2+r_3-r_1)+\arg(\mathcal{R})\right] + \left(\frac{r_2+r_3}{r_1|\mathcal{R}|}\right)\csc\left[k(r_2+r_3-r_1)+\arg(\mathcal{R})\right]\right\} \tag{11b}$$

The phase change also depends on all the three distances, on the modulus and argument of the reflection factor, and on the frequency of the waves. In the particular case of the receiver near the ground, when $r_1 = r_2 + r_3$, and the ground does not change the phase of the wave, $\arg(\mathcal{R}) = 0$, there is not any phase change due to the presence of the reflected wave.

3 Model II for multiple paths in mountainous terrain

The extension to non-flat ground (Figure 3) requires knowledge of the terrain profile

$$z = h(x) \tag{12}$$

in the plane of the line-of-sight.

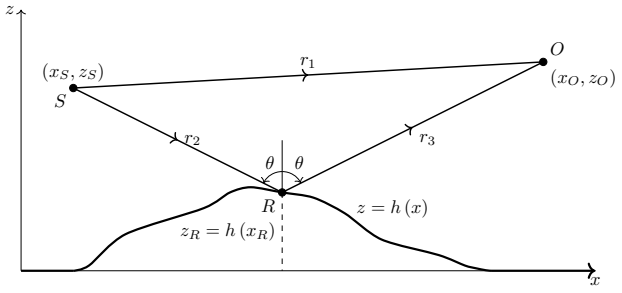

Figure 3: As in Figure 2 over rough ground with a given altitude profile in two dimensions.

Taking into account one wave that can reflect on the ground and reaches the observer's position, the formulas for the reflected (5) and hence for the total (8) acoustic pressure, due to one wave originated from the source, can also be used in the model II. In this model, the pressure perturbation represents again a wave with outward spherical propagation centred at the source and depends only on the radial distance from it. Therefore, the harmonic solutions (5) and (8), using again the principle of superposition, remain valid as solutions of the linearised wave equation, deduced from the same assumptions, and do not depend on the terrain profile.

Although the distance r_1 remains valid in the model II, the ray distances r_2 and r_3 that also appear in the previously mentioned equations cannot be calculated in the same way than in the model I because those expressions consider the terrain profile depicted in the Figure 2, valid only if the ground is flat. To calculate the two ray distances (6) and (7), the coordinates of the reflection point are necessary. The difference from the case of flat ground is that the location of the reflection point is no longer given by the Eqs. (3) or (4), because the reflection point is no longer at zero height:

$$R \mapsto (x_R, h(x_R)) . \tag{13}$$

Thus, the condition (3) is replaced (Figure 3) by

$$\frac{z_O - h(x_R)}{x_O - x_R} = \cot\theta = \frac{z_S - h(x_R)}{x_R - x_S} \tag{14a}$$

that states again the equality of the angles of incidence and reflection asserted by the Snell's law of specular reflection. In (14a), the terms dependent on the reflection point x_R are separated on the right-hand side:

$$\frac{x_O z_S + x_S z_O}{z_O + z_S} = x_R + \frac{x_O + x_S - 2x_R}{z_O + z_S} h(x_R) . \tag{14b}$$

Given the source $S \equiv (x_S, z_S)$ and observer $O \equiv (x_O, z_O)$ positions, the solutions of the Eq. (14b) for x_R give the reflection point(s) in the plane of line-of-sight. For flat ground, $h(x_R) = 0$, there is only one solution, given explicitly by (4). For rough ground there may be several x_{R_j} reflection points R_j, with $j = 1, \ldots, M$, depending on the terrain profile (12). Then, by knowing the coordinates of the reflection point(s), the ray distances r_{2_j} from source S to reflection point R_j and r_{3_j} from reflection point R_j to observer O can be calculated for each reflection point in the same way than in the Eqs.(6) and (7), but substituting z_S and z_O respectively by $z_S - h(x_{R_j})$ and $z_O - h(x_{R_j})$ because in this model the coordinates of the reflection points are now given by (13). However, Eq. (14b) is not the most accurate to determine the coordinates of reflection points in such a way that the wave, after the reflection on the ground, reaches the observer's position. The equality of the angles in (14a) was made regarding the geometric characteristics of the Figure 3 and with the application of the Snell's law, asserting that the angles of incidence and reflection have the same value in which they are measured from the correspondent wave to the normal of the ground; however, as highlighted in the Figure 3, it is assumed in (14b) that the normal to the surface lies in vertical (in the z direction), and the latter may not be exactly perpendicular to the ground. This simplification that will be retained in the remainder of the paper under the assumption that the slope of the terrain is neglected,

$$\left(\frac{\mathrm{d}h}{\mathrm{d}x}\right)^2 \ll 1,$$

yields that the angles of incidence and reflection are still measured from a vertical normal direction.

The total sound field,

$$p_{II} = \frac{\mathrm{e}^{\mathrm{i}kr_1}}{r_1} + \sum_{j=1}^{M} \mathcal{R}_j \frac{\mathrm{e}^{\mathrm{i}k\left(r_{2_j} + r_{3_j}\right)}}{r_{2_j} + r_{3_j}}, \tag{15}$$

is similar to Eq. (8) with a sum over all the reflection points, where the reflection factor $\mathcal{R}_j$ may vary with the reflection point, whereas r_{2_j} and r_{3_j} are the distances from the source and observer, respectively, to the j-th reflection point. The effect on the acoustic energy is obtained substituting (15) in the Eq. (9),

$$E_{II} = \left|\frac{p_{II}}{p_0}\right|^2 = \left|1 + \sum_{j=1}^{M} \mathcal{R}_j \frac{r_1}{r_{2_j} + r_{3_j}} \mathrm{e}^{\mathrm{i}k\left(r_{2_j} + r_{3_j} - r_1\right)}\right|^2 , \tag{16a}$$

or the change of SPL on a decibel scale,

$$\begin{aligned} A_{II} &\equiv 10\log E_{II} \qquad (16b)\\ &= 10\log\left\{1+\sum_{j=1}^{M}\left(\frac{r_1}{r_{2_j}+r_{3_j}}\right)^2\left|\mathcal{R}_j\right|^2\right.\\ &+2\sum_{j=1}^{M}\frac{r_1\left|R_j\right|}{r_{2_j}+r_{3_j}}\cos\left[k\left(r_{2_j}+r_{3_j}-r_1\right)+\arg\left(\mathcal{R}_j\right)\right]\\ &+2\sum_{j=1}^{M}\sum_{l=1}^{j-1}\frac{r_1}{r_{2_j}+r_{3_j}}\frac{r_1}{r_{2_l}+r_{3_l}}\left|\mathcal{R}_j\right|\left|\mathcal{R}_l\right|\cos\left[k\left(r_{2_j}\right.\right.\\ &\left.\left.+\ r_{3_j}-r_{2_l}-r_{3_l}\right)+\arg\left(\mathcal{R}_j\right)-\arg\left(\mathcal{R}_l\right)\right]\Bigg\}. \end{aligned}$$

Since the last summation varies from $l = 1$ to $j - 1$, then when $j = 1$, it yields zero leading back to Eq. (10b). The change of phase of the acoustic pressure perturbation,

$$\Phi_{II} = \arg\left(p_{II}\right) - \arg\left(p_0\right) = \operatorname{arccot}\left[\frac{\operatorname{Re}\left(p_{II}/p_0\right)}{\operatorname{Im}\left(p_{II}/p_0\right)}\right], \quad (17a)$$

is given by

$$\begin{aligned} \Phi_{II} = \operatorname{arccot}\Bigg\{&\left(1+\sum_{j=1}^{M}\left|\mathcal{R}_j\right|\frac{r_1}{r_{2_j}+r_{3_j}}\cos\left[k\left(r_{2_j}\right.\right.\right. \qquad (17b)\\ &\left.\left.\left.+\ r_{3_j}-\ r_1\right)+\arg\left(\mathcal{R}_j\right)\right]\right)\left(\sum_{j=1}^{M}\left|\mathcal{R}_j\right|\frac{r_1}{r_{2_j}+r_{3_j}}\times\right.\\ &\left.\sin\left[k\left(r_{2_j}+r_{3_j}-r_1\right)+\arg\left(\mathcal{R}_j\right)\right]\right)^{-1}\Bigg\}. \end{aligned}$$

In the case of a single reflection point $j = l = M = 1$, then the Eqs. (16b) and (17b) reduce respectively to the equations of the model (10b) and (11b). In this model, there can be more than one reflected wave reaching the observer's position and all these waves influence the multipath factor, that is, it is a result of the combination of all these waves (superposition principle). The amplitude and phase of the acoustic pressure perturbation induced by the reflected waves when they reach the final position depend on how far they travel, on their frequencies (although the frequency of all reflected waves is the same) and on the reflection coefficient at each reflection point; fundamentally, they depend on the coordinates of each reflection point. Since these coordinates are functions of the ground profile, in order to predict a final result from the superposition of all the reflected waves besides the direct wave, the ground profile must be known accurately. In an hypothetical situation when the ray distance of all the reflected waves is equal to the ray distance of the direct wave (the real situation is $r_2 + r_3 > r_1$), the change in SPL or in phase do not depend on the frequency of the waves and if moreover the reflection coefficient is unit throughout the ground, then $A_{II} = 10\log(1+M)^2 = 20\log(1+M)$ (when $M = 1$, there is one reflected wave and the increase of SPL would be 6.02 dB). It follows from the Eq. (16a), and considering a constant reflection coefficient, that the reflected waves which have a greater influence on the multipath factor are the waves that propagate a shorter distance $r_2 + r_3$. Hence, if there is a reflected wave that propagates a much smaller distance than the others, the problem of several reflected waves can be simplified to the case of model I: besides the direct wave, the existence of the reflected wave that propagates the smallest distance.

4 Model III for the effects of atmospheric attenuation

It is assumed that the atmosphere is homogeneous and at rest, so that the attenuation $\delta(r)$ depends only on the distance of propagation, *viz.* Eq. (8) is replaced by

$$p_{III} = \frac{\mathrm{e}^{\mathrm{i}kr_1-\delta_1}}{r_1} + \mathcal{R}\frac{\mathrm{e}^{\mathrm{i}k(r_2+r_3)-\delta_2-\delta_3}}{r_2+r_3} \qquad (18)$$

where in the case of uniform atmospheric absorption per unit length, $\varepsilon = \text{const.}$, the attenuations are given by

$$\{\delta_1,\delta_2,\delta_3\} = \varepsilon\{r_1,r_2,r_3\}. \qquad (19)$$

The effect of ground reflection,

$$p_{III} = \frac{\mathrm{e}^{\mathrm{i}kr_1-\delta_1}}{r_1}F, \qquad (20)$$

is equivalent to the multiplication by a factor

$$F = 1 + \mathcal{R}G, \qquad (21a)$$

that differs from unity on account: (i) of the geometrical factor

$$G \equiv \frac{r_1}{r_2+r_3}\mathrm{e}^{\mathrm{i}k(r_2+r_3-r_1)+\delta_1-\delta_2-\delta_3}, \qquad (21b)$$

that depends only on observer and source positions; (ii) of the reflection factor $\mathcal{R}$, that depends on ground properties. The effect on acoustic energy (9) is now

$$\begin{aligned} E_{III} &= \left|\frac{p_{III}\mathrm{e}^{\delta_1}}{p_0}\right|^2 = \left|1+\mathcal{R}G\right|^2 \qquad (22a)\\ &= \left|1+\mathcal{R}\left(\frac{r_1}{r_2+r_3}\right)\mathrm{e}^{\mathrm{i}k(r_2+r_3-r_1)+\delta_1-\delta_2-\delta_3}\right|^2, \end{aligned}$$

i.e. the change in SPL is

$$A_{III} = 10\log E_{III} \tag{22b}$$
$$= 10\log\left\{1 + \left(\frac{r_1}{r_2+r_3}\right)^2 |\mathcal{R}|^2\, \mathrm{e}^{2\delta_1-2\delta_2-2\delta_3} + 2\frac{r_1}{r_2+r_3}|\mathcal{R}|\,\mathrm{e}^{\delta_1-\delta_2-\delta_3}\cos\left[k\left(r_2+r_3-r_1\right) + \arg\left(\mathcal{R}\right)\right]\right\}.$$

As in the model I, the amplitude change depends on all the three ray distances, on the frequency of the waves and on the reflection coefficient. However, in this model, it also depends on the three attenuations. The particular case of receiver near the ground, $O \equiv R$, when the distances travelled by the reflected and direct waves are exactly the same, $r_1 = r_2 + r_3$, leads to a similar result to model I with a correction for attenuation $G = \exp(-\delta_1)$, that is $p_r = \mathcal{R}Gp_0$; the same correction applies to the direct wave, $p_0 \to p_0 G$, implying for the total wave $p_{III} = (1+\mathcal{R})\,Gp_0$. If the definition for case I is used where the atmospheric attenuation is not considered in the direct wave, $E_{III} = |p_{III}/p_0|^2$, consequently the SPL in decibels changes by $10\log\left\{1 + |\mathcal{R}|^2 G^2 + 2|\mathcal{R}|\,G\cos\left[\arg\left(\mathcal{R}\right)\right]\right\}$. Therefore, if both waves travel the same distance, the multipath factor does not depend on the frequency, except possibly through the attenuation factor that generally increases with frequency. In the case $\arg(\mathcal{R}) = 0$, the change of SPL reduces to $20\log\{1 + |\mathcal{R}|\,G\}$ and if the boundary totally reflects the wave, $|\mathcal{R}| = 1$, the total acoustic pressure perturbation changes by $20\log(1+G)$, and in the presence of atmospheric attenuation $G < 1$ this is less than $20\log 2 = 6$ dB. That attenuation does not alter the fact that the observer receives two waves of the same frequency, amplitude and phase (doubling the incident wave) when the ground does not change none of the characteristics of the wave and the distance travelled by both waves is the same. Therefore, if the correct definition of SPL changes for the case III is used, $E_{III} = \left|p_{III}\mathrm{e}^{\delta_1}/p_0\right|^2$, then the total acoustic pressure perturbation changes by $20\log 2 = 6$ dB when the boundary totally reflects the wave, $\mathcal{R} = 1$.

The change in phase of the acoustic pressure perturbation is

$$\Phi_{III} = \arg\left(\frac{p_{III}\mathrm{e}^{\delta_1}}{p_0}\right) \tag{23}$$
$$= \operatorname{arccot}\left\{\cot\left[k\left(r_2+r_3-r_1\right) + \arg\left(\mathcal{R}\right)\right] + \frac{r_2+r_3}{r_1|\mathcal{R}|}\mathrm{e}^{\delta_2+\delta_3-\delta_1} \times \csc\left[k\left(r_2+r_3-r_1\right) + \arg\left(\mathcal{R}\right)\right]\right\}.$$

It also depends on all the three ray distances, on the modulus and argument of the reflection factor, on the frequency of the waves and, in this model, on all the three attenuations. As in the first model, in the particular case when $r_1 = r_2 + r_3$ and the ground does not change the phase of the wave, $\arg(\mathcal{R}) = 0$, there is not any phase change due to the presence of the reflected wave.

In the absence of atmospheric attenuation, $\delta_1 = \delta_2 = \delta_3 = 0$, then Eqs. (22b) and (23) reduce respectively to Eqs. (10b) and (11b).

The simplest form of the reflection coefficient $\mathcal{R}$ [10] is

$$\mathcal{R} = \frac{1-\mathcal{R}_0}{1+\mathcal{R}_0}, \tag{24}$$

for an homogeneous ground of density ρ_1, generally much higher than the air density ρ_0,

$$\mathcal{R}_0 = \frac{\rho_0\kappa'}{\rho_1\kappa}, \tag{25}$$

where: (i) the vertical wavenumbers of incidence κ and transmission κ' are given respectively by

$$\kappa = \frac{\omega}{c_0}\cos\theta \tag{26a}$$

and

$$\kappa' = \frac{\omega}{c_1}\cos\theta'; \tag{26b}$$

(ii) c_0 and c_1 are the sound speeds in air and ground respectively; (iii) the angles of incidence θ and transmission θ' are related by Snell's law

$$\frac{\sin\theta}{c_0} = \frac{\sin\theta'}{c_1}, \tag{27}$$

stating the continuity of the transverse wavenumber. Substituting the Eq. (27) in (26a) and (26b), and then into (25) leads to

$$\mathcal{R}_0 = \frac{\rho_0 c_0}{\rho_1 c_1}\sqrt{\sec^2\theta - \left(\frac{c_1}{c_0}\right)^2\tan^2\theta}, \tag{28}$$

which specifies the reflection factor (24) in terms of the angle θ in the relations (3) and (14a). In (28) appears the ratio of plane wave impedances of air $\rho_0 c_0$ and ground $\rho_1 c_1$.

5 Determination of the coordinates of reflection points

The study of the effects caused by ground reflection and atmospheric absorption on aircraft noise depends on the location of the reflection point(s). The latter affects the length

of the ray paths, and hence, since the multipath factor depends on all the distances, the amplitude decays and phase shifts due to the atmosphere and ground profile. The location of the reflection point(s) is calculated in the cases of: (i) flat ground; (ii) two-dimensional slice of rough ground.

5.1 Reflection from flat ground

Each of the three ground reflection and atmosphere models mentioned in the introduction, and in particular the two presented here, leads to a formula for the effects of ground reflection and atmospheric absorption on the total acoustic pressure perturbation p, that specifies: (i) the difference in acoustic energy or difference in SPL in dB,

$$A = 10 \log_{10} |E| = 20 \log_{10} \left| \frac{p}{p_0} \right| ; \tag{29}$$

(ii) the phase shift of the acoustic pressure

$$\Phi = \arg \left(\frac{p}{p_0} \right) = \arg (p) - \arg (p_0) . \tag{30}$$

Since the pressure perturbations are harmonic solutions that are functions of the ray distances, these outputs depend on the calculation of the reflection point(s). Before proceeding in the sequel to reflections on rough ground, first the simplest case of flat ground is considered, that applies to the models I and III, for which there is a single reflection point.

The source $S \equiv (X_S, Y_S, Z_S)$ and observer $O \equiv (X_O, Y_O, Z_O)$ positions are given (Figure 4). Their horizontal projections are at distance d; the line joining the horizontal projections makes an angle ϕ with the X-axis. If the ground is flat, the only single reflection point is on a vertical plane that contains the source and observer points, between both positions. That means the only reflected wave that arrives at the observer position travels only on that plane. All other

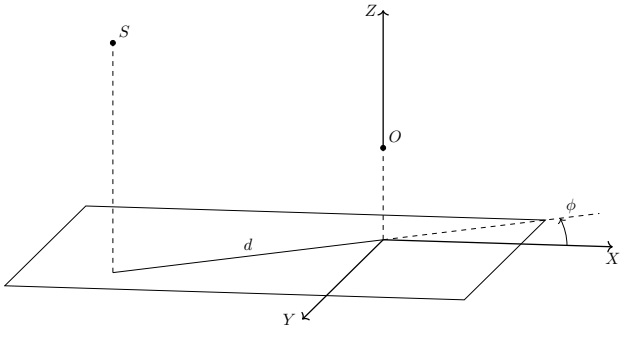

Figure 4: Relative positions of source and observer over a flat ground as in Figure 2.

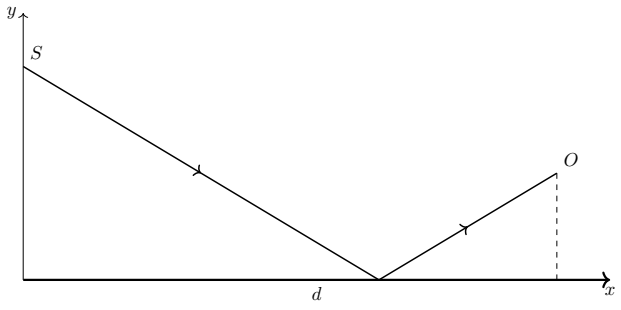

Figure 5: Two-dimensional slice in the vertical plane through source and observer in the case of flat ground.

waves (moving out of the vertical plane) will not reach the observer position. Therefore, in this case, we can reduce the problem to two dimensions. Making a section by a vertical plane passing through the source and observer positions (Figure 5) and choosing Cartesian coordinates with Ox-axis on the ground and Oy-axis passing through the source, lead to the coordinates in the source-observer reference system:

$$x_S = 0, \quad y_S = Z_S, \tag{31}$$

for the source and

$$y_O = Z_O, \quad x_O = d \equiv \left| (X_S - X_O)^2 + (Y_S - Y_O)^2 \right|^{1/2} \tag{32}$$

for the observer. The location of the reflection point and the effects on acoustic energy follow as in (4) for the model I and for its extension to include atmospheric absorption in the model III.

5.2 Two-dimensional slice of rough ground

Let the height of the rough ground be given by

$$Z = H (X, Y) . \tag{33}$$

The two-dimensional slice (Figure 5) made as before leads for an arbitrary point $P \equiv (X, Y, Z)$ to an x- coordinate in the source-observer coordinate system,

$$x = \left| (X - X_O)^2 + (Y - Y_O)^2 \right|^{1/2} , \tag{34}$$

and the angle ϕ with the x-axis,

$$\tan \phi = \frac{Y - Y_O}{X - X_O} . \tag{35}$$

Using the transformation

$$X = X_S + x \cos \phi , \tag{36a}$$

$$Y = Y_S - x \sin \phi , \tag{36b}$$

the two-dimensional slice through the rough ground is specified in the source-observer coordinate system by

$$y = h(x) = H(X_S + x\cos\phi, Y_S - x\sin\phi). \quad (37)$$

This specifies the terrain profile function (12) used in the model II.

6 Application of the three models of ground and atmospheric effects

The method of application is similar for all the preceding three models presented in this paper, allowing for rough, irregular or mountainous ground with a given profile and including or not atmospheric absorption. The simplest ground profiles are: (i) flat ground, e.g. with arbitrary impedance; (ii) undulating ground, e.g. a sinusoid with given height and wavelength.

6.1 General method to determine the multipath factor

The steps in the solution procedure, valid for any of the three preceding models, are as follows:

1. input the source and observer positions;
2. in the case of flat ground use Eqs. (31) and (32) to locate the reflection point (4), or in the case of uneven ground (33), construct the two-dimensional slice by a vertical plane (37) using Eqs. (34) to (36b), and determine the reflection points as solutions of (14b);
3. from each reflection point, calculate the distances to source (6) and observer (7);
4. calculate the reflection factor from (24) and (28) for hard ground, or take from the literature relevant to the particular type of ground being considered;
5. the expression of the total acoustic pressure perturbation is different in the three models, knowing however that the pressure induced by the direct wave, $p_0 = \exp(\mathrm{i}kr_1 - \delta_1)/r_1$ is the same:
   (a) the effect of reflection at one point on a flat ground is then given by (8) in the model I;
   (b) taking a constant atmospheric absorption per unit length ε leads to an extension to (18) in the model III;
   (c) in the case of reflection at a discrete set of points over mountainous terrain, the effect of all reflections is considered in (15) by the model II, where the correction for the atmospheric absorption can be included as before in (18);
6. all the previous three forms of E lead to an amplitude (29) and a phase changes (30) combining all effects of ground reflection and atmospheric absorption, knowing that the total acoustic pressure perturbation p is equal to p_I, p_{II} or p_{III} respectively for the models I, II or III.

As an application to the preceding theories including the calculation of reflection points, the case of static source and observer in fixed positions over flat ground, applying the model I, is considered, and then extended to sinusoidally undulating ground, applying the model II, or extended to include atmospheric absorption, applying the model III. The standard case is the sound source in a fixed position at the altitude of 30 m *viz.*

$$Z_S = 30\,\mathrm{m}, \quad (38)$$

while the observer, for instance a human being, is at 2 m above a flat ground,

$$Z_O = 2\,\mathrm{m}. \quad (39)$$

The comparison is made with sinusoidally undulating ground

$$Z_r = h(X_r) = q\sin\left(\frac{2\pi X_r}{L}\right), \quad (40)$$

with amplitude q and lengthscale L:

$$q = 3\,\mathrm{m} \quad L = 20, 40, 60, \infty\,\mathrm{m}. \quad (41)$$

The case $L = \infty$ is flat ground, and the others lead to a maximum slope

$$\theta_{\max} = \arctan\left(\frac{2\pi q}{L}\right). \quad (42)$$

In addition, three levels of atmospheric absorption,

$$\varepsilon = 10^{-2}, 5\times10^{-2}, 10^{-1}\,\mathrm{m}^{-1}, \quad (43)$$

are considered to apply the model III. The levels of atmospheric absorption in (43) vary widely, in order to make the effects visible. The case of undulating ground is preceded by comparison with flat ground.

6.2 Acoustic waves over flat impedance ground

The preceding methods are illustrated by applying the models I and III to fixed sound sources over a flat impedance

ground. The model I is illustrated in Figure 6 for sound source, $S \mapsto (x_S, z_S)$, and observer, $O \mapsto (x_O, z_O)$, at positions (38) and (39) over a flat ground. The sound attenuation (that is, the SPL variation) and the phase shift of acoustic pressure perturbation are shown for a rigid ground $\mathcal{R} = 1$ or for a ground with reflection coefficient $\mathcal{R} = 0.5 + 0.5\mathrm{i}$, for a horizontal distance between the source and observer $x = x_O - x_S = 50\,\mathrm{m}$, for a source at a height of $z_S = 30\,\mathrm{m}$, and for an observer at a height of $z_O = 2\,\mathrm{m}$. Because the ground remains flat the multipath factor does not depend on the particular values of horizontal coordinates of observer and source, x_S and x_O, but only on their difference $x = x_O - x_S$. Thus (x_O, x_S) appear only through x and together with the vertical coordinates of source z_S and observer z_O specify the lengths of the ray paths $r_1 = \left|x^2 + (z_O - z_S)^2\right|^{1/2}$, $r_2 = z_S\left[1 + x^2/(z_O + z_S)^2\right]^{1/2}$ and $r_3 = z_O\left[1 + x^2/(z_O + z_S)^2\right]^{1/2}$. These last three expressions were deduced with the Eq. (4) that is valid only for flat ground. In the example of Figure 6 (for $\mathcal{R} = 1$, top), the distances are almost equal, $r_1 = 57.31\,\mathrm{m}$ whereas $r_2 + r_3 = 59.36\,\mathrm{m}$, and therefore the successive peaks in the upper left plot correspond to 5.86 dB, very close to 6.02 dB. In summary, when the waves with the same frequency are in phase, a condition that depends on both ray paths and the wavenumber k, the total amplitude reaches a maximum (constructive interference). Besides that, the value of that maximum amplitude depends on the factor $r_1/(r_2 + r_3)$ and only in the particular situation when $r_1 = r_2 + r_3$ it reaches the highest possible value: twice the amplitude of the direct wave, leading to $A_I = 6.02\,\mathrm{dB}$. On the other hand, the successive minimum values on the plot correspond to waves that are in opposite phases, and in the specific example of Figure 6 (upper left figure), these minimums have the value −29.21 dB. The lowest possible value occurs if the waves are in the opposite phase (that depends on both ray distances and the wavenumber k) and if $r_1 = r_2 + r_3$, where there is a total cancellation of them, $p_I = 0$, leading to a theoretical value of $A_I = -\infty\,\mathrm{dB}$. All the ray paths are even functions with respect to x and their values don't change if one permutes the z_O and z_S values. Consequently, the multipath factor and subsequent plots will be the same if one switches the positions of observer and source.

The perfect interference of direct and reflected waves for rigid ground (Figure 6, top left) leads to maxima of almost double amplitude and minima of almost zero amplitude. When two waves superpose, it can form a total wave of greater, lower or same amplitude. Suppose that the two waves (direct and reflected on the ground) have the same amplitude and frequency along their ray paths,

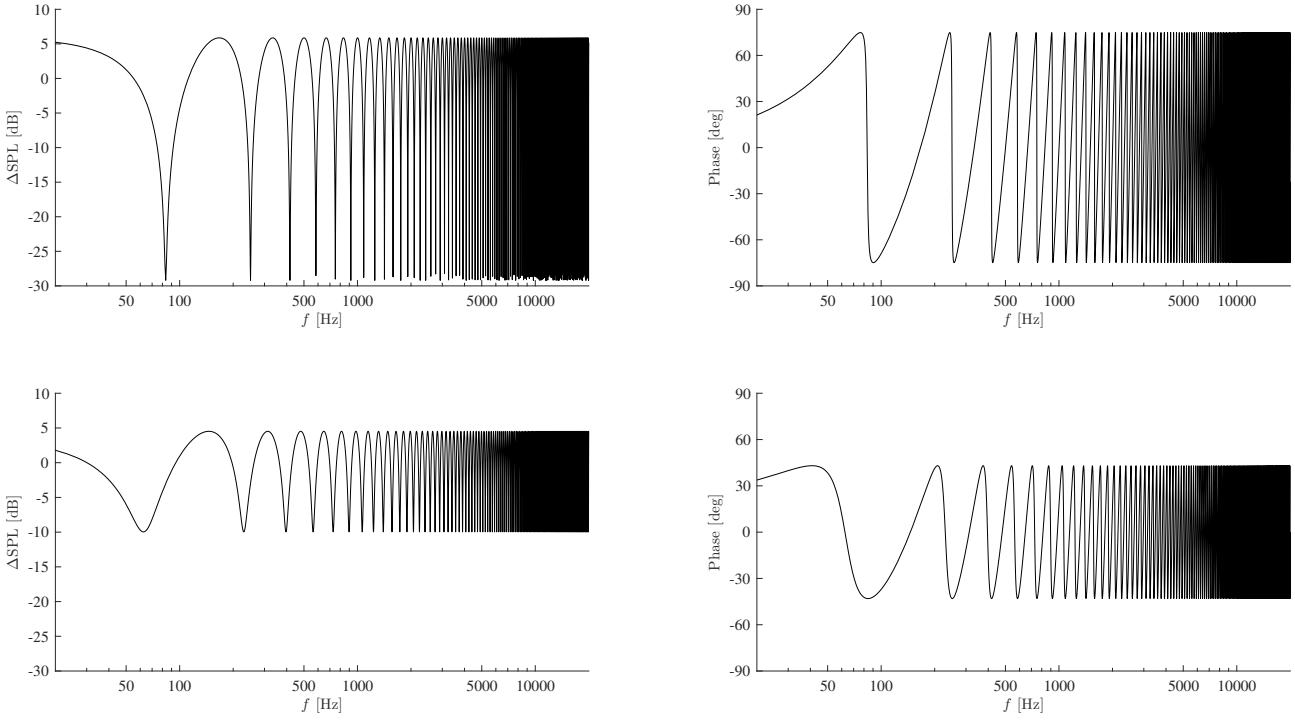

Figure 6: Sound attenuation and phase shift of the acoustic pressure for a ground reflection $\mathcal{R} = 1$ (top) or $\mathcal{R} = 0.5 + 0.5\mathrm{i}$ (bottom), a horizontal distance between source and observer $x = x_O - x_S = 50\,\mathrm{m}$, a source at a height of $z_S = 30\,\mathrm{m}$, and an observer at a height of $z_O = 2\,\mathrm{m}$, as functions of sound frequency.

and reach the observer's position. To simplify, consider first the case of $\mathcal{R} = 1$ (Figure 6, top) when the phase and the complex amplitude of the wave are not changed when it impinges on the surface. One extreme case is the constructive interference when at the observer's point the phase difference between the two waves is an even multiple of π ($\ldots, -2\pi, 0, 2\pi, \ldots$) or, equivalently, when the difference between the ray distances of both waves is an integer multiple of the wavelength. Consequently, $k(r_2 + r_3 - r_1) = 2\pi n$ (n is an integer) and A_I is maximum. Note that when the distances travelled by both waves are exactly the same, $r_2 + r_3 - r_1 = 0$, the conditions are satisfied too. One can check the validity of these observations in (10b) because when that happens, the cosine function in the equation is equal to one and the value of A_I is maximum. Respecting these conditions, the two waves are in phase but it doesn't mean that the amplitude of the sum of both waves is twice the amplitude of the direct wave. Consider, for instance, $k(r_2 + r_3 - r_1) = 0$, but the ray distances are different, $r_1 < r_2 + r_3$ (for geometric reasons, it is impossible to have $r_1 > r_2 + r_3$). As explained before, in that case the waves are in phase, hence the value of A_I is maximum. Nevertheless, because the waves are spherical, the complex amplitude of the acoustic pressure perturbation is directly proportional to $1/r$ where r is the distance travelled by the wave. Therefore, since $r_1 < r_2 + r_3$, the complex amplitude of p_r is lower than p_0, or the complex amplitude of $p_I = p_r + p_0$ is lower than $2p_0$, and consequently A_I is lower than $20\log 2 = 6.02$ dB (we are summing two waves with same frequency, in phase, but of different amplitudes). One can have the same conclusion through the Eq. (10b) with $\mathcal{R} = 1$, $r_1 < r_2 + r_3$ and $k(r_2 + r_3 - 1) = 2\pi n$ and noting that $A_I < 10\log 4 = 6.02$ dB. The other extreme case is the destructive interference when at the observer's point the phase difference between the two waves is an odd multiple of π ($\ldots, -3\pi, -\pi, \pi, 3\pi, \ldots$) or, equivalently, when the difference between the ray distances of both waves is an integer plus one-half multiple of the wavelength. In that case, $k(r_2 - r_3 - r_1) = (\pi + 2\pi n)$, the cosine function in (10b) is zero and A_I is minimum. Additionally, if the two waves have the same amplitude, A_I is $-\infty$ dB, however that only happens if the sum of both waves is zero and that is only possible, due to their spherical propagations, if $r_1 = r_2 + r_3$ (when the waves have the same complex amplitudes). In this study, we always have $r_2 + r_3 > r_1$, therefore the complex amplitudes are different and then, even when they are in opposite phases, the sum is not zero, but it can be almost zero (resulting in negative minimums of A_I). The bottom left plot of the Figure 6 shows the effect of varying the value $\mathcal{R}$ on the SPL values, keeping constant the positions of observer and source. According to (10b), there are two independent effects of changing $\mathcal{R}$ on SPL plots, one caused by changing its complex magnitude and another by its phase: its phase influences the positions of maximum and minimum values, in other words, keeping constant the positions of observer and source, it determines the values of frequency in which the two waves are in phase or in opposite phase, for instance if $\arg(\mathcal{R}) > 0$, the extreme values occur at lower frequencies in comparison when $\arg(\mathcal{R}) = 0$; the complex magnitude of $\mathcal{R}$ changes only the values of maxima and minima of A_I. Then, when $\mathcal{R}$ changes from 1 to $0.5 + 0.5\mathrm{i}$, the extreme values of A_I will be lower in modulus and will occur at lower frequencies.

The extremes presented in the upper left plot of Figure 6 correspond to zeros of the function in the upper right one. When a crest of a wave meets a crest of another wave of the same frequency at the same point (constructive interference) or when a crest of one wave meets a trough of another wave (destructive interference), the phase of total wave will be equal to the phase of direct wave, therefore $\Phi_I = 0$ in (11a). Considering the first equality of (8), and the condition that the incident waves are in phase, $\arg(p_0) = \arg(p_r) + 2\pi n$, then

$$|p_I|\, \mathrm{e}^{\mathrm{i}\arg(p_I)} = (|p_0| + |p_r|)\, \mathrm{e}^{\mathrm{i}\arg(p_0)} \tag{44}$$

implying that the phase of total wave remains the same while its complex magnitude is the sum of magnitudes of both incident waves. If the waves are in opposite phases, $\arg(p_0) = \arg(p_r) + \pi + 2\pi n$, the phase of the total wave would be also equal to the phase of the direct wave because

$$\begin{aligned} |p_I|\, \mathrm{e}^{\mathrm{i}\arg(p_I)} &= |p_0|\, \mathrm{e}^{\mathrm{i}\arg(p_0)} + |p_r|\, \mathrm{e}^{\mathrm{i}\arg(p_r)} \\ &= (|p_0| - |p_r|)\, \mathrm{e}^{\mathrm{i}\arg(p_0)}, \end{aligned} \tag{45}$$

taking into account that $|p_r| = |\mathcal{R}| / (r_2 + r_3) < |p_0| = 1/(r_1)$ and therefore the expression in curved parentheses is equivalent to $|p_I|$ while $\arg(p_0) = \arg(p_I)$. The Eq. (11b) leads to the same conclusion: when the phase of the waves differ by a multiple of π, $k(r_2 + r_3 - r_1) + \arg(\mathcal{R}) = n\pi$, then $\cot(n\pi)$ and $\csc(n\pi)$ are (both positive or negative) infinities and consequently (with the sum of positive or negative infinities being equal to positive or negative infinity respectively) the arccotangent function approaches to zero (in either cases). In summary, the constructive or destructive interferences of the two waves correspond to zeros of the plots of phase change. The bottom right plot of Figure 6 shows the effect of varying the value of $\mathcal{R}$ in the phase of multipath factor. As in the plots of the complex magnitude, there are also two independent effects: the phase of $\mathcal{R}$ determines the frequencies that correspond to zeros (relating to constructive and destructive interferences), maxima and minima of phase Φ_I, for instance, increasing the phase of $\mathcal{R}$, like from

1 to 0.5 + 0.5i, in Figure 6, reduces the frequencies of zeros and extreme values of Φ_I as one can compare in the right plots; the complex magnitude of $\mathcal{R}$ influences the range of phase values of Φ_I, for instance, the effect of decreasing $|\mathcal{R}|$ is to reduce the extreme values of phase of the multipath factor and the right plots of Figure 6 show that changing the value of $\mathcal{R}$ from 1 to 0.5 + 0.5i (hence reducing the complex magnitude of $\mathcal{R}$) shrinks the range of phase values of the multipath factor. One can infers the same conclusions analysing mathematically the Eq. (11b).

As shown in Figure 6, the maximum and minimum extremes are more closely spaced for higher frequencies, both for amplitude (left plots) and phase (right plots), but it happens only because the independent axis is in a logarithmic scale. Actually, the extremes remain equally spaced for higher frequencies. The ground with complex reflection coefficient (Figure 6, bottom) smooths out the maxima and minima, leading to a smaller range of amplitudes (bottom left) and phases (bottom right). Although the Figure 6 shows the SPL and phase changes for a certain reflection coefficient and for certain positions of receptor and source, the plots would be similar (a succession of equally spaced crests and troughs) for other values of the aforementioned parameters, and with the maximum theoretical SPL change also being equal to 6.02 dB. The differences would be in the range of the SPL and phase values, and also in the frequencies corresponding to crests or troughs because the positions of constructive or destructive interference would be shifted.

The frequency as independent variable in Figure 6 is replaced by observer height z_O, source height z_S and observer-source distance x respectively in Figures 8, 9 and 10. The plots of Figure 6 show that the modulus (left plots) and phase (right plots) oscillations have extreme amplitudes with the same value independently of frequency (changing the frequency only leads to different positions where extreme amplitudes take place), therefore the subsequent plots are set for one frequency, $f = 1$ kHz. However, the values of extreme amplitudes of the multipath factor depend on the other three parameters: (i) increasing the observer height (Figure 8) decreases the amplitude of intensity (top) and phase (bottom) oscillations; (ii) increasing the source height (Figure 9) does not affect the amplitude but increases the spacing of extrema of intensity (top) and phase (bottom) oscillations; (iii) increasing the observer-source distance (Figure 10) affects both the spacing and amplitude of intensity (top) and phase (bottom) oscillations. For all the plots from Figures 8 to 10, two geometrical parameters are fundamental to analyse them: the difference of ray lengths, $r_2 + r_3 - r_1$ and also their ratio, $r_1/(r_2 + r_3)$. The plots of these two parameters are shown in Figure 7 to help to understand the multipath factor effects.

Considering z_O as independent variable, the maxima and minima of SPL changes (Figure 8, top) are related to

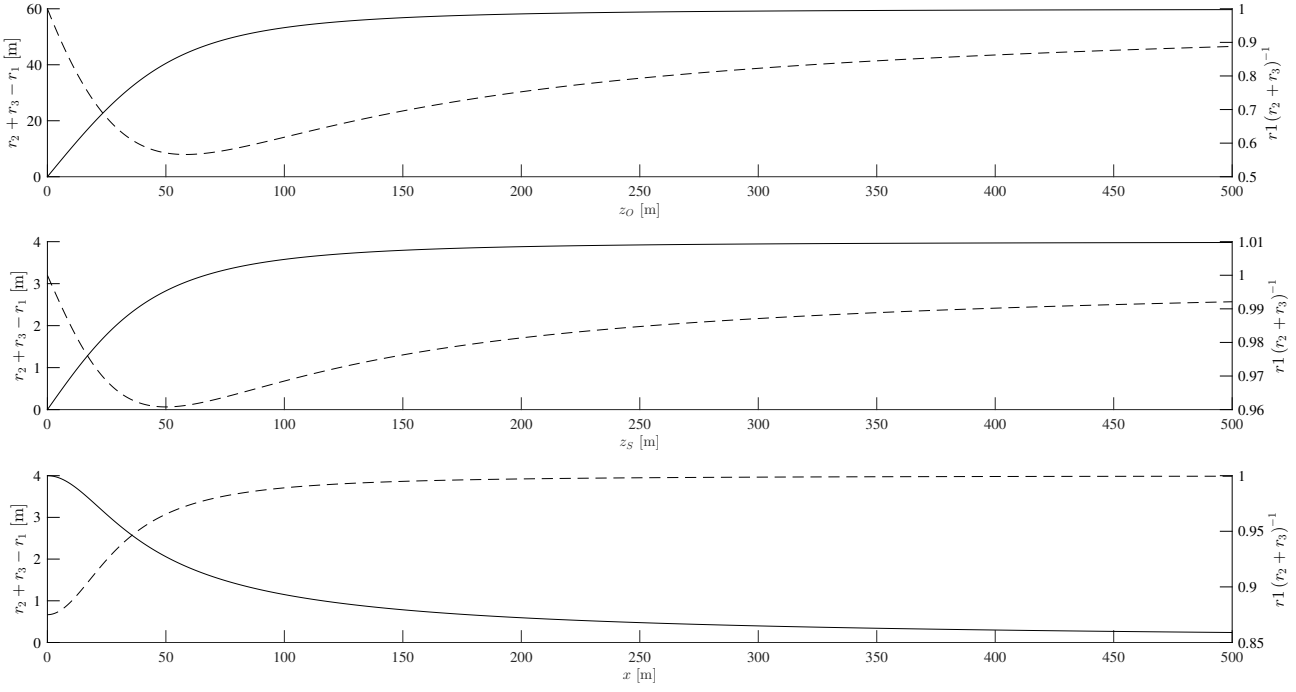

Figure 7: Geometrical parameters $r_2 + r_3 - r_1$ (continuous line) and $r_1/(r_2 + r_3)$ (dashed line) plotted for $z_O = 2$ m, $z_S = 30$ m and $x = 50$ m case, but where each one of them is assumed as independent variable.

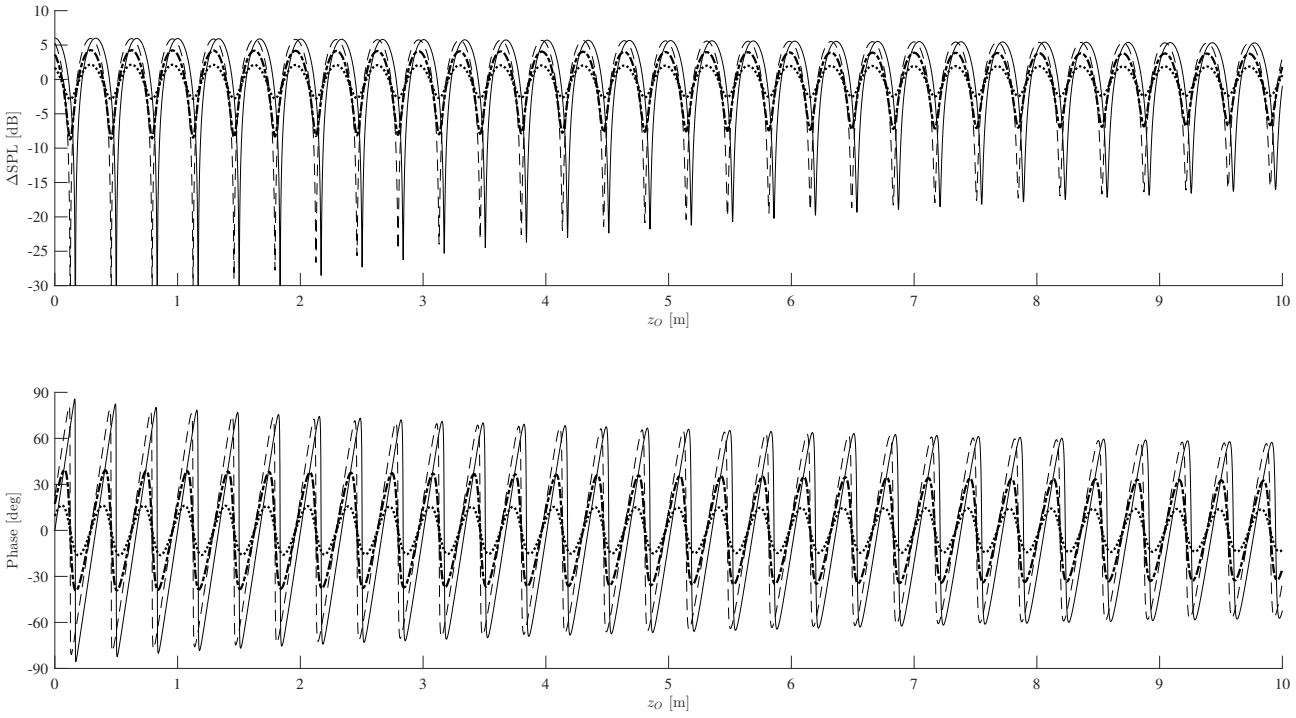

Figure 8: Sound attenuation and phase shift as functions of observer height z_O, for flat hard ground with $\mathcal{R} = 1$ (solid line) or for semi-flat grounds with $\mathcal{R} = 0.7 + 0.7\mathrm{i}$ (dashed line), $\mathcal{R} = 0.45 + 0.45\mathrm{i}$ (dash-dot line) and $\mathcal{R} = 0.2 + 0.2\mathrm{i}$ (dotted line). The sound frequency is $f = 1\,\mathrm{kHz}$, the observer is at a horizontal distance $x = 50\,\mathrm{m}$ from the source, and the source is at a height $z_S = 30\,\mathrm{m}$.

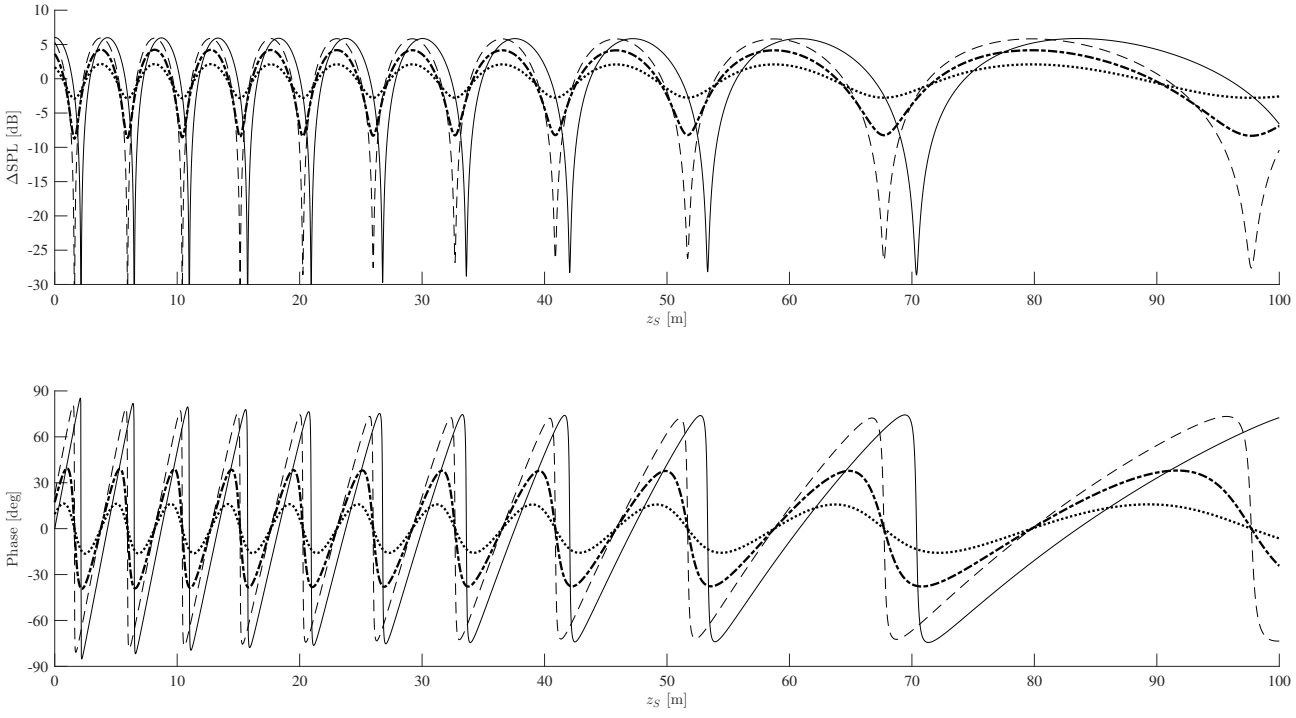

Figure 9: Sound attenuation and phase shift as functions of source height z_S, for flat hard ground with $\mathcal{R} = 1$ (solid line) or for semi-flat grounds with $\mathcal{R} = 0.7 + 0.7\mathrm{i}$ (dashed line), $\mathcal{R} = 0.45 + 0.45\mathrm{i}$ (dash-dot line) and $\mathcal{R} = 0.2 + 0.2\mathrm{i}$ (dotted line). The sound frequency is $f = 1\,\mathrm{kHz}$, and the observer is at a horizontal distance $x = 50\,\mathrm{m}$ from the source and at a height $z_O = 2\,\mathrm{m}$.

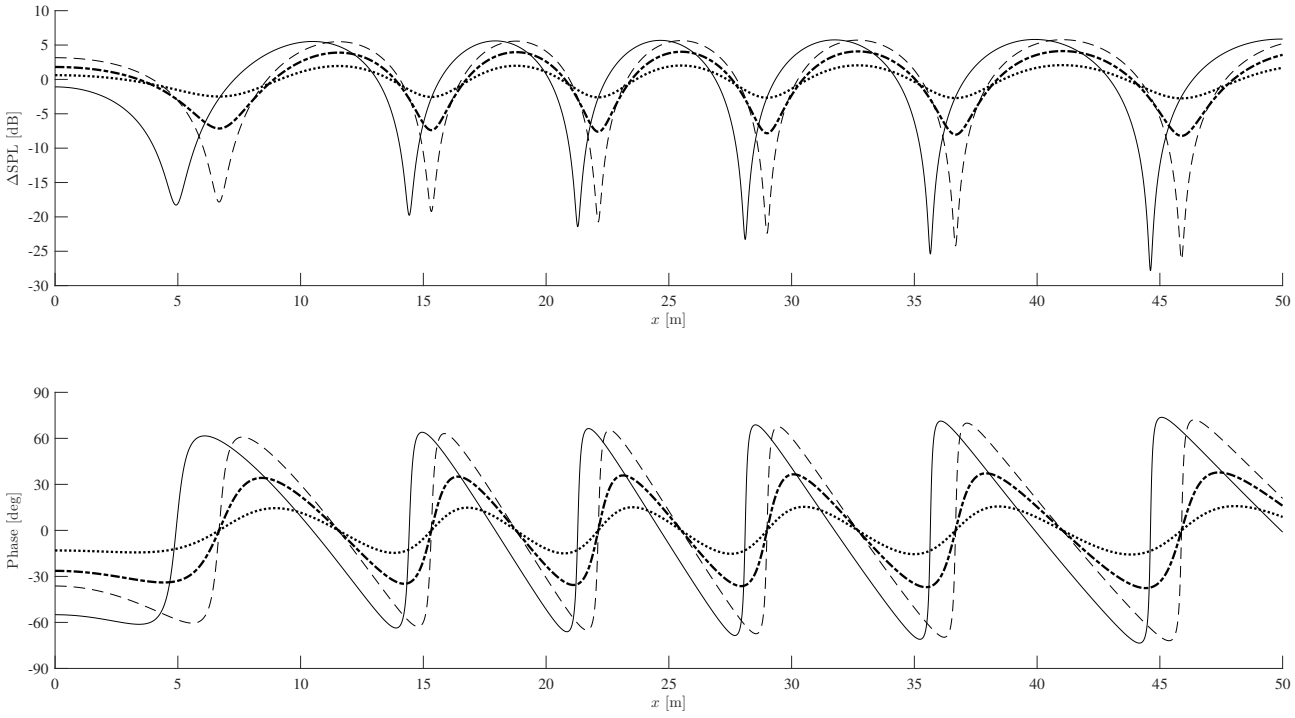

Figure 10: Sound attenuation and phase shift as functions of observer-source distance x, for flat hard ground with $\mathcal{R} = 1$ (solid line) or for semi-flat grounds with $\mathcal{R} = 0.7 + 0.7\mathrm{i}$ (dashed line), $\mathcal{R} = 0.45 + 0.45\mathrm{i}$ (dash-dot line) and $\mathcal{R} = 0.2 + 0.2\mathrm{i}$ (dotted line). The sound frequency is $f = 1\,\mathrm{kHz}$, the observer is at a height $z_O = 2\,\mathrm{m}$, and the source is at a height $z_S = 30\,\mathrm{m}$.

constructive and destructive interferences respectively and, regarding (10b), the cosine function must be equal to one in modulus. To simplify, consider $\mathcal{R} = 1$. In the case of constructive interference, setting the cosine function to one (when the cosine function is one, we are analysing the maximum values of A_I), although the three ray distances depend on z_O, the factor $\mathfrak{r} = r_1/(r_2 + r_3)$ is a monotonic decreasing function until 10 meters at least (this fact is demonstrated in the top plot of Figure 7) and consequently the term in bracket parentheses of (10b), equal to $(1 + \mathfrak{r})^2$, decreases with z_O. Hence, the successive peaks of A_I slightly monotonically decrease with z_O. On the other hand, in the case of destructive interference, when the cosine function is equal to minus one (hence analysing the minimum values of A_I), the term in bracket parentheses reduces to $(1 - \mathfrak{r})^2$, that increases with z_O (because the variable $\mathfrak{r}$ is decreasing), and consequently the successive minimum values of A_I also increase, as shown in the top plot of Figure 8. Actually, the effect of varying z_O is more noticeable in the increasing of minima than in decreasing of maxima of A_I. The reason is because of the logarithm effect in (10b) where the logarithm function changes quicker near the abscissa 0 (when the term in bracket parentheses is almost 0, a phenomenon of destructive interference) than in abscissa greater than 1 (when the term in bracket parentheses is almost 4, a phenomenon of constructive interference). These interpretations also explain the behaviour of extremes in the bottom plot of Figure 8 because, as indicated in (11b), the parameter $r_1/(r_2 + r_3)$ also appears in the equation and is useful to understand that plot. The phase space between maxima, minima or zeros of both plots in Figure 8 is almost constant because $r_2 + r_3 - r_1$ behaves approximately like z_O for small values of z_O (note the almost proportional behaviour between z_O and $r_2 + r_3 - r_1$ in the top plot of Figure 7 for $z_O < 25\,\mathrm{m}$), then the cosine function can be simplified to $\cos(kz_O)$ in (10b) and the same thing for the phase plot in (11b) when the argument of the trigonometric functions is also reduced to kz_O.

The same reasoning can be applied to Figures 9 and 10. Assuming z_S as independent variable in Figure 9, the middle plot in Figure 7 is important in this case. When $z_S < 25\,\mathrm{m}$, according to the plot, one can approximate the difference of ray paths $r_2 + r_3 - r_1$ as $0.08z_S$ and because of the cosine function presented in (10b), the space between the extrema is much larger in Figure 9 than in 8. Furthermore, that space in Figure 9 is increasing with z_S, specifically for $z_S > 25\,\mathrm{m}$, because the derivative of $r_2 + r_3 - r_1$ with respect to z_S is lowering and consequently the cosine function behaves like $\cos(kaz_S)$ with $a < 0.08$, hence the space between the extrema starts to increase in comparison

with the space for $z_S < 25$ m (and as a consequence, also the space between the zeros of the function Φ_I in Figure 9). On the other hand, the values of the maxima and minima of the functions A_I and Φ_I, mainly the former one, remain approximately constant because the ratio between ray paths, $r_1 (r_2 + r_3)^{-1}$, also remains approximately constant with z_S as one can observe from the middle dashed plot in Figure 7. In the case of bottom plot of Figure 7, for $x < 50$ m, the derivative of the continuous line starts to decrease, reaches a constant negative value and then begins to increase, therefore the space between the extrema points in top and bottom plots and the space between the zeros in bottom plot, both of Figure 10, follow the same pattern as the change of the derivative aforementioned (the space starts to decrease until a certain point, then remains constant and finally the space increases). Moreover, for $x < 50$ m, the dashed line in the bottom plot of Figure 7 monotonically increases (instead of the dashed lines of other plots in Figure 7), hence the maximum values increase while the minimum values decrease with x (because of the logarithm function, the effect is more noticeable in the minimum values). Note that the increasing/decreasing the values of extrema points is more visible in the Figure 8 than in Figures 9 and 10 due to a wider range of values of the parameter $r_1/(r_2 + r_3)$, as one can observe from a comparison between the ranges of the dashed lines in the Figure 7.

Figures 7 to 10 show the plots for certain positions of observer and source and for a certain frequency. However, independently of that values, the SPL and phase changes depend always on the parameters $r_2 + r_3 - r_1$ and $r_1 (r_2 + r_3)^{-1}$. If one changes the positions of the observer and source, the shapes of the curves shown in the Figure 7 would be similar. For instance, in the top plot of the Figure 7, the parameter $r_2 + r_3 - r_1$ would continue to monotonically increase while the parameter $r_1 (r_2 + r_3)^{-1}$ would continue to form an U-shaped curve (however, the minimum of the value would shift its abscissa). The differences would be in the range of the values of both parameters. For instance, keeping $x = 50$ m, if $z_O = 50$ m, the parameter $r_2 + r_3 - r_1$ increases from 0 to 100 meters while the parameter $r_1 (r_2 + r_3)^{-1}$ is between 0.4 and 1; otherwise, if $z_O = 95$ m, the parameter $r_2 + r_3 - r_1$ increases up to 190 meters while the parameter $r_1 (r_2 + r_3)^{-1}$ is between 0.25 and 1. Moreover, keeping constant the value $z_S = 30$ m, if $x = 5$ m, the parameter $r_1 (r_2 + r_3)^{-1}$ varies between 0.08 and 1, but if $x = 95$ m, the parameter $r_1 (r_2 + r_3)^{-1}$ varies between 0.73 and 1; however, if x changes while the heights of the source z_S and receptor z_O are constant, the parameter $r_2 + r_3 - r_1$ has the same range of values. In all these cases, the shapes of the curves of both parameters remain the same; consequently, the plots of the Figure 8 would have the same shape, with a succession of crests and troughs, with the parameter $r_2 + r_3 - r_1$ controlling the spacing between the "waves" of the plots and with the parameter $r_1 (r_2 + r_3)^{-1}$ controlling the amplitude of that "waves". Besides, in most of the cases, the maximum SPL increase is between 5 and 6 decibels. Regarding the middle plots of the Figure 7, changing the value of x or z_O, the range of values of the parameters $r_2 + r_3 - r_1$ and $r_1 (r_2 + r_3)^{-1}$ would also change. The only exception is the parameter $r_2 + r_3 - r_1$ remaining constant when one changes the horizontal distance x, keeping constant the other values. Nevertheless, the shape of both curves in the middle plot of the Figure 7 is the same: the parameter $r_2 + r_3 - r_1$ monotonically increases while the parameter $r_1 (r_2 + r_3)^{-1}$ forms an U-shaped curve (but the minimum of the curve changes its abscissa). Therefore, the conclusions about the Figure 9 hold for different coordinates of the observer and source, and even for a different frequency (but can have different amplitudes and different spacing between the "waves"). All previous observations are the same for the bottom plot of the Figure 7. Changing the heights of the receptor z_O and source z_S will change the values of both aforementioned parameters (however, when only the height of the source z_S or only the height of the observer z_O changes, keeping constant the other values, not only the range but also the format of the curve of the parameter $r_2 + r_3 - r_1$ remain the same, provided that the condition $z_S \geq z_O$ is checked), but in the other side the format of both curves will be kept (a S-curved shape for $r_1 (r_2 + r_3)^{-1}$ and an inverted S-curved shape for $r_2 + r_3 - r_1$). Consequently, the spacing of the "waves" and their amplitudes in the Figure 10 will show the same trends while x increases for different values of the other parameters.

All the plots from Figures 8 to 10 show also the effects of $\mathcal{R}$ on the multipath factor. The interpretation mentioned to explain the Figure 6 can be used to explain Figures 8 to 10. Comparing the continuous with dashed lines in Figures 8 to 10, one can observe the effect of changing the phase of $\mathcal{R}$ because the complex magnitudes of $\mathcal{R}$ for both lines are almost the same: 1 and 0.99. Since $\arg(\mathcal{R})$ only appears in the arguments of trigonometric functions in the Eqs. (10b) and (11b) respectively for the modulus and phase plots, increasing the phase of $\mathcal{R}$ only shifts the extreme points and zeros to the left or right and the plots do not move vertically, while increasing its complex magnitude also increases the values of the extreme points. Comparing the dashed line with the dash-dot and dotted lines in Figures 8 to 10 shows the effects of varying only the value $|\mathcal{R}|$ because the phase of $\mathcal{R}$ is exactly the same between the three lines. Looking at the ΔSPL plots, resulting from the Eq. (10b), one can conclude that the decrease in the value of $|\mathcal{R}|$ leads only to a vertical shrink of the values in that

plots, therefore the extremes values decrease in modulus, but do not translate them horizontally, consequently the zeros and extrema points remain at the same abscissas; increasing the complex magnitude of $\mathcal{R}$ leads to the opposite effect since it only extends vertically the plots. The effect of translating vertically the plots due to a change in $|\mathcal{R}|$ is also visible in the bottom plots of Figures 8 to 10, but it is not the only one. Decreasing the complex magnitude also shifts right or left the plots of Φ_I (bottom plots) because $|\mathcal{R}|$ appears in the arccotangent function, but doesn't shift horizontally the plots of A_I (top plots). Therefore, since the extrema points of A_I have the same abscissas when one changes only the complex magnitude of $\mathcal{R}$ (because that plots do not not move horizontally), the zeros of Φ_I (in bottom plots) remain at the same coordinates because that points and the extrema points of A_I have always the same abscissas.

Knowing the effects of all coordinates (z_S, z_O, x) and reflection coefficient $\mathcal{R}$ on the multipath factor, the atmospheric attenuation can now be discussed to understand how it influences also the multipath factor. Considering in this paper the simplest case, when the atmospheric attenuation has spherical symmetry and depends only on the distance of propagation, as stated in the assumption (19), the only important parameter to consider is the difference of ray distances between the direct and reflected waves, $r_2+r_3-r_1$. In the formulas of the multipath factor for the model III, (22b) and (23) for its complex magnitude and phase respectively, the three attenuations $(\delta_1, \delta_2, \delta_3)$ appear in the equations merely in the form $\exp[-\varepsilon(r_2 + r_3 - r_1)]$ with $\varepsilon \geq 0$. Starting from $\varepsilon = 0$, the exponential function reduces to 1 and therefore the multipath factor will be equal to that of model I, with no attenuation. If one increases the value of ε, or in other words increasing the strength of atmospheric attenuation, and plots the data as a function of some distance, like it was done in the Figures 8 to 10, the results would be very similar to the plots shown in that figures and it would be observed that increasing ε leads to a smaller range (a vertical shrink of the plots) of SPL and phase values, similar to the effect of decreasing $|\mathcal{R}|$ that is visible in the previously mentioned figures. Indeed, increasing ε or decreasing $|\mathcal{R}|$ weakens the strength of the signal received at the observer position, the first due to an atmospheric absorption and the last due to a creation of a transmitted wave from the surface with $|\mathcal{R}| < 1$ when the incident wave impinges on it. Note that to effectively shrink the plots of the multipath factor, in the last case, a sufficient condition is the ground not being acoustically hard, $|\mathcal{R}| < 1$; however, in the former case, it is not sufficient to have some atmospheric attenuation because to shrink the plots, the reflected wave must be more attenuated than the direct wave, that is, $\delta_2 + \delta_3 > \delta_1$ (in the simplified case of uniform attenuation, this is always verified since $r_2 + r_3 > r_1$). One additional remark has to be considered: when $r_2 + r_3 = r_1$, since both waves travel the same distance and consequently suffer the same "amount" of uniform atmospheric attenuation, the multipath factor is not modified when that attenuation is considered. Indeed, the atmospheric effect is less visible when both ray distances tend to be very similar because in that particular circumstance the direct and reflected waves are almost equally attenuated due to the atmosphere and therefore the SPL and phase changes tend to be equal to the changes with no atmospheric attenuation. Mathematically, when $r_2 + r_3 \to r_1$, then the SPL change approaches the result of the model I (with no atmospheric attenuation), $A_{III} \to A_I$, and the same consequence to the phase change, $\Phi_{III} \to \Phi_I$. These consequences are valid for any reflection factor and positions of observer and source. Therefore, one can know when the difference of ray paths is approximately zero by following the continuous lines of Figure 7 and consequently, for that combination of values of x, z_S and z_O (to determine the difference $r_2 + r_3 - r_1$) one can predict that the atmospheric attenuation (mainly to small values of ε) changes only slightly the multipath factor. Moreover, the constructive and destructive interferences do not depend on the atmospheric attenuation, that is, the extreme points of the complex magnitude (and consequently the zeros of the phase) of the multipath factor remain at the same abscissas because the attenuations only influence the amplitudes of waves and not their phases of propagation. Indeed, according to (22b), the attenuation parameter does not appear in the cosine argument which is the responsible term for the location of the extreme points of the SPL plots (and zeros of the phase plots).

The effect of atmospheric absorption (Figure 11) is equally noticeable for the intensity (top) as for the phase (bottom) of the multipath factor. The lines are plotted for the next case: the ground is acoustically hard, $\mathcal{R} = 1$, the heights of the observer and source are respectively 2 and 30 meters, while they are 50 meters apart, and the frequency of the waves is 1 kHz. However, each line represents a variation of one single value from the default case, which is represented by the thinner solid line. The line type specifies which variable (except the frequency) has its value changed from the default set, and for the same type, each line thickness has a different value of the variable concerned. All these changes are pointed out in the Table 1 to clarify the meaning of each line in the Figures 11 and 12. Independently of the geometrical parameters, reflection coefficient of the ground and frequency of the waves, when the atmospheric attenuation is very small, that is, when is negligible, the SPL and phase changes are almost equals to the changes

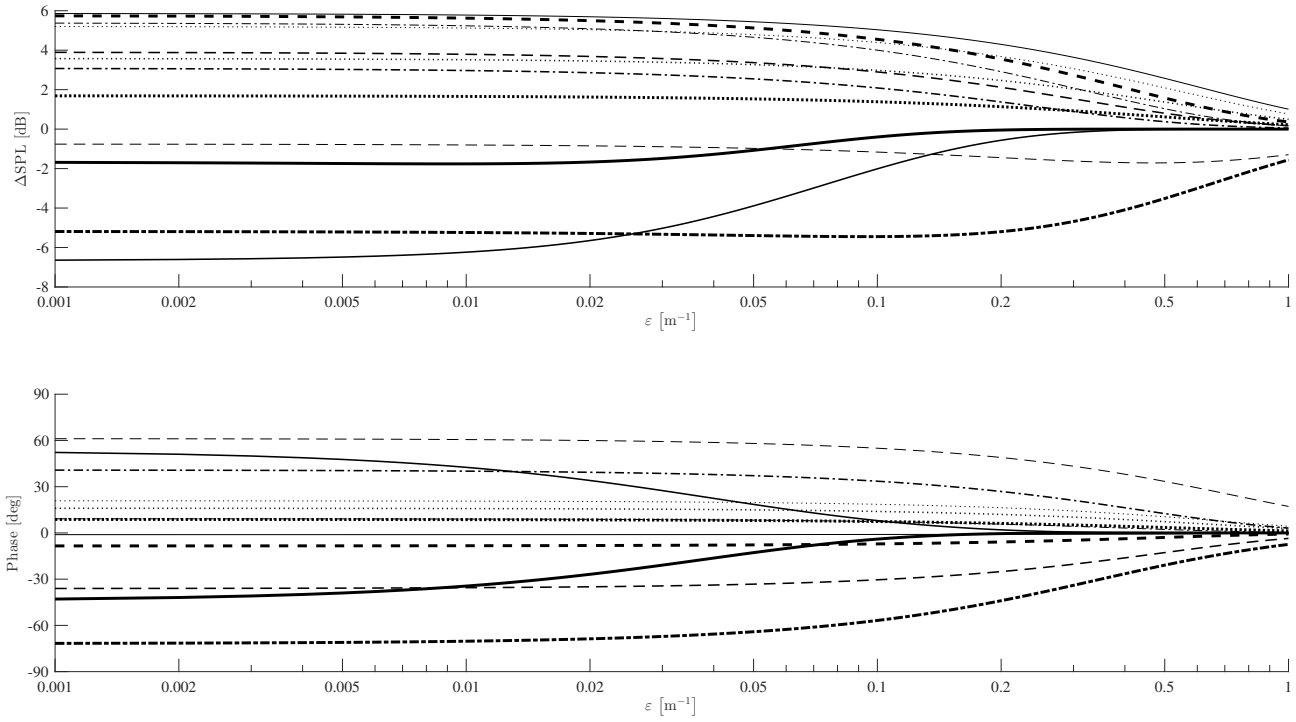

Figure 11: Sound attenuation and phase shift due to ground effect as functions of atmospheric absorption per unit length ε, where the default case (solid thinner line) is for hard ground $\mathcal{R} = 1$, the sound frequency $f = 1$ kHz, the observer at a height $z_O = 2$ m, the source at a height $z_S = 30$ m and at a distance of $x = 50$ m from the observer. Each line represents a variation of one single value aforementioned and it is indicated in Table 1.

Table 1: List of the cases for each line in both plots of Figures 11 and 12. The default case is the next set of values: $\{z_O, z_S, x, \mathcal{R}\} = \{2, 30, 50, 1\}$ corresponding to the thinner solid line.

Line type	Line thickness		
	Thinner	Normal	Thicker
Solid	$z_O = 2$ m	$z_O = 12$ m	$z_O = 22$ m
Dashed	$z_S = 15$ m	$z_S = 45$ m	$z_S = 60$ m
Dotted	$x = 10$ m	$x = 30$ m	$x = 70$ m
Dash-dot	$\mathcal{R} = 0.7 + 0.7$i	$\mathcal{R} = 0.45 + 0.45$i	$\mathcal{R} = 0.2 + 0.2$i

if the attenuation is not included in the calculus; when $\varepsilon \to 0$, then $A_{III} \to A_I$ and $\Phi_{III} \to \Phi_I$. By looking at the plots in Figure 11, the attenuation effect becomes important when $\varepsilon > 0.02\,\mathrm{m}^{-1}$. However, the importance of atmospheric attenuation is influenced not only by the value of ε, but also by the difference of ray paths, $r_2 + r_3 - r_1$. As the uniform atmospheric attenuation is considered, if that difference is small, both waves are attenuated with the same intensity and the only difference between these waves and the waves with no attenuation is that the former ones reach the observer's position with lower amplitudes, but at the same ratio between the direct and reflected waves; that is, mathematically when $r_2 + r_3 - r_1 \to 0$, then $|p|_{\mathrm{dir.I}} / |p|_{\mathrm{refl.I}} = |p|_{\mathrm{dir.III}} / |p|_{\mathrm{refl.III}}$ with $|p|_{\mathrm{dir.III}} < |p|_{\mathrm{dir.I}}$ and $|p|_{\mathrm{refl.III}} < |p|_{\mathrm{refl.I}}$, where dir. and refl. stand for direct and reflected waves respectively, while I and III stand for the models I (without attenuation) and III (with attenuation). Consequently, in that situation, the results approach also the ones of the model I. To summarize, the fundamental parameter that influences the multipath factor is $\varepsilon\,(r_2 + r_3 - r_1)$ and the effects of atmosphere become negligible for small values of that parameter. On the other hand, when the atmospheric absorption increases, the SPL and phase changes tend to be almost zero, independent of the difference of ray paths. That happens because for large atmospheric absorptions, in the general case of $r_2 + r_3 > r_1$, the reflected wave is much more attenuated (because it travels a larger distance) than the direct wave, and hence the total wave

received at the observer's position is reduced to the direct wave only, $p_{III} \approx p_0 \exp(-\delta_1)$; mathematically, for bigger ε, then $\exp[-\varepsilon(r_2 + r_3 - r_1)] \to 0$, consequently $A_{III} \to 0$ and $\Phi_{III} \to \operatorname{arccot}\{\cot[k(r_2 + r_3 - r_1) + \arg(\mathcal{R})]\}$.

The difference in intensity with and without atmospheric attenuation (Figure 12) increases sharply as the latter exceeds about $0.02\,\mathrm{m}^{-1}$, at least, for all cases mentioned in the Table 1. The figure reinforces the interpretation that in these cases, for $\varepsilon < 0.02\,\mathrm{m}^{-1}$, the difference is insignificant, since the SPL changes of the models I and III (with and without atmospheric attenuation) are almost equal. The difference starts to increase when $\varepsilon > 0.02\,\mathrm{m}^{-1}$. That difference can be positive or negative, depending on the geometrical parameters, the reflection coefficient and the frequency of waves. When $\varepsilon \sim 1\,\mathrm{m}^{-1}$, the waves are strongly attenuated by the atmosphere, with the reflected wave much more attenuated than the direct wave, since $r_2 + r_3$ is greater than r_1, and usually $A_{III} \sim 0\,\mathrm{dB}$, (for instance, in all the cases of Table 1 we have $-1.56\,\mathrm{dB} < A_{III} < 1.01\,\mathrm{dB}$). Consequently, the difference can be simplified to merely $-A_I$ and therefore can be predicted by the results of model I. In Figure 12, there are three cases of positive differences when $\varepsilon > 0.02\,\mathrm{m}^{-1}$, $A_{III} - A_I \approx -A_I > 0$, because A_I is negative in all those situations; in other cases, the difference is negative because A_I is positive in that situations (except for the dashed thinner line where A_{III} is "more" negative than A_I; the attenuation shrinks vertically the SPL plots, but the intersection between the plots with $\varepsilon = 0$ and $\varepsilon = 1$ do not occur when SPL is 0 dB). To predict the signal of the values of A_I, the reader can analyse the top plots of Figures 8 to 10 to observe when A_I is positive or negative, and read the discussion about model I.

The conclusions about the Figures 11 and 12 hold for other values of the parameters, including not only the coordinates of the observer and source, but also the frequency. Nevertheless, the effect of atmospheric attenuation, or equivalently the difference between the SPL change with and without atmospheric absorption $A_{III} - A_I$, can be significant from a value of ϵ less than $0.02\,\mathrm{m}^{-1}$.

Understanding the influence of ε and its related parameters on the SPL and phase plots, one can now analyse the plots of the difference in intensity with and without atmospheric absorption as a function of some geometrical parameters (as it was done in the Figures 8 to 10), for instance, of the observer distance (Figure 13). The plots show peaks at the locations of the destructive interference, because the latter is less effective in the presence of attenuation. As discussed before, since the positions of destructive

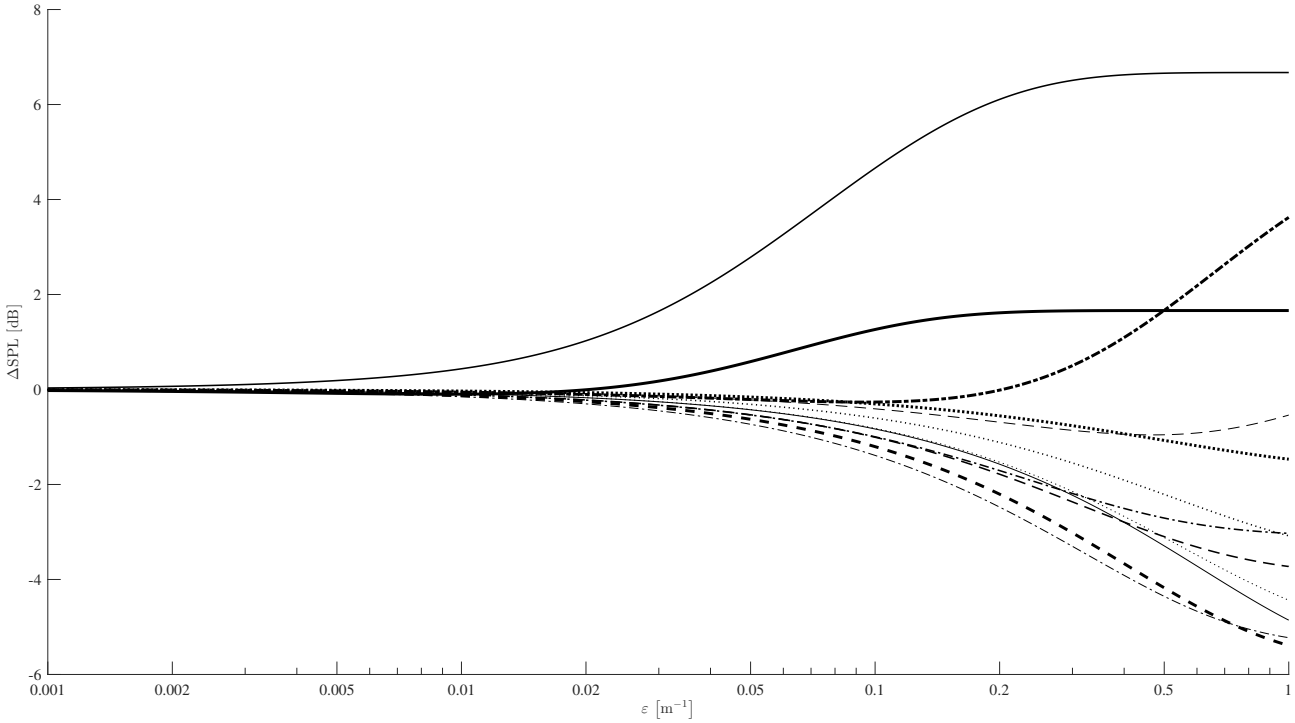

Figure 12: Difference between sound attenuation due to ground effect with and without atmospheric absorption, $A_{III} - A_I$, as a function of atmospheric absorption per unit length ε, where the default case (solid thinner line) is for hard ground $\mathcal{R} = 1$, sound frequency $f = 1\,\mathrm{kHz}$, observer at a height $z_O = 2\,\mathrm{m}$, source at a height $z_S = 30\,\mathrm{m}$ and at a distance of $x = 50\,\mathrm{m}$ from the observer. Each line represents a variation of one single value aforementioned, in the same way as in the Figure 11, and that variation is indicated in Table 1.

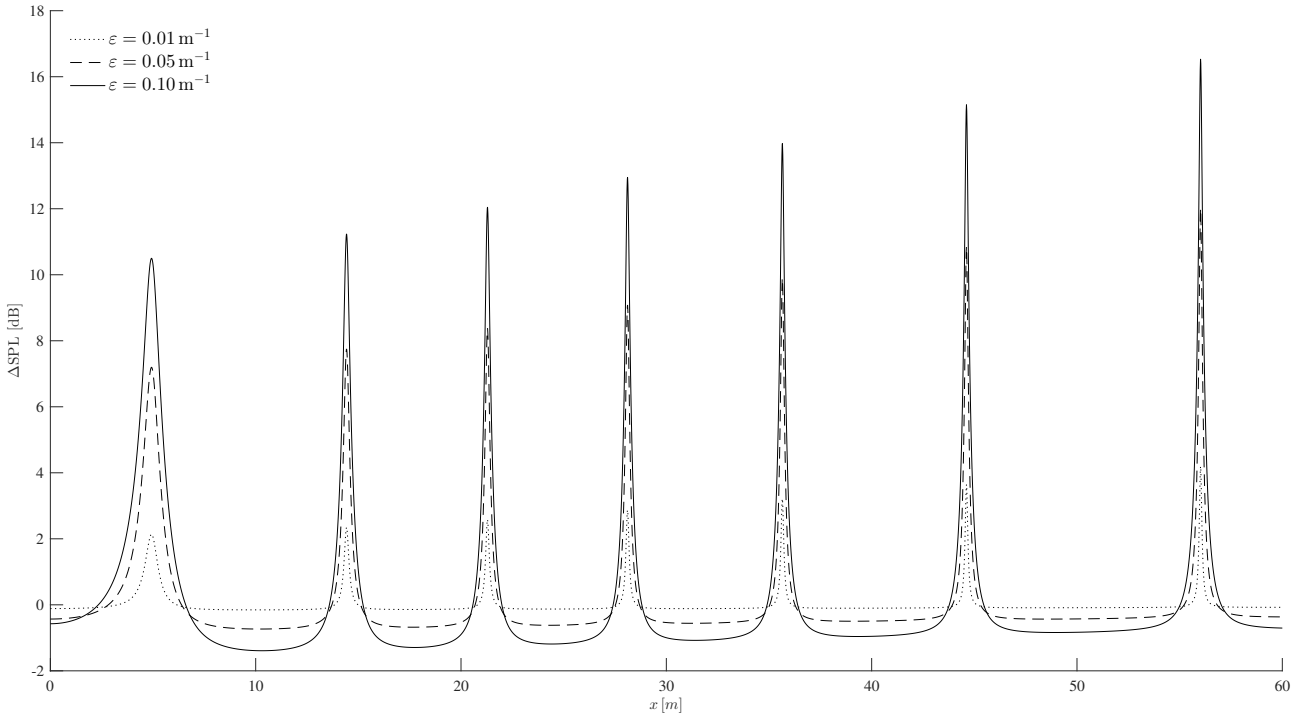

Figure 13: Difference between sound attenuation due to ground effect with and without atmospheric absorption for three values of ε and for hard ground $\Re = 1$, as a function of the distance between source and observer. The sound frequency is $f = 1$ kHz, the observer is at a height $z_O = 2$ m, and the source is at a height $z_S = 30$ m.

interference are not influenced by the presence of atmospheric attenuation nor its value (it is influenced mainly by the difference of ray paths and frequency of the waves), the peaks of the Figure 13 occur at the same values of x, independent of the value of ε. In the Figure 13, one can observe that, for $\varepsilon = 0.1\,\mathrm{m}^{-1}$, the presence of attenuation can lead to an increase of 16 dB. However, that is not a problem for the noise monitoring because those maximum increases occur always at the positions of total destructive interferences, where A_I is, at least, lower than -15 dB (see the top plot of Figure 10), and consequently A_{III}, that considers the atmospheric attenuation, never reaches a positive value at the positions of peaks shown in the Figure 13. On the other hand, the minimum values of the Figure 13 occur at the positions of constructive interferences. In those positions, both A_I and A_{III} are positive values, but A_{III} is lower than A_I, hence resulting in negative differences shown in the Figure 13. Indeed, as mentioned before in this section 6, the presence of ε shrinks the plots of SPL changes and therefore the maximum values of SPL with atmospheric attenuation are lower than the maximum values without attenuation and, on the other hand, the minimum values of SPL with attenuation are higher than the minimums without attenuation (equivalently, A_{III} is lower than A_I in modulus). The graphs in Figure 13 are plotted assuming x as the independent variable, however the graphs and the discussion would be similar if one assumes z_S or z_O as independent variable rather than x, because the atmospheric attenuation always shrinks the plots of SPL changes. These conclusions hold not only for other values of the coordinates of observer and source, but also for other values of the frequency. However, it is possible that in a specific case the minimum value of the plot reach a value less than –1 decibel as shown in the Figure 13 (for instance, increasing the observer's height z_O to 80 meters, the minimum value of the plot reaches less than –4 decibels; the lowest theoretical minimum would be –6.02 decibels when the atmospheric attenuation is high enough to attenuate totally the reflected wave, A_{III} is equal to 0, and consequently the difference $A_{III} - A_I$ is equal to $-A_I = -6.02$ dB in the positions of total constructive interference).

6.3 Effect of undulating ground compared with flat ground

To study the effects of undulating ground on the multipath factor, the model II is illustrated for a terrain profile specified by a continuous function with a continuous derivative, of which the sine function is a good example to represent

an undulating ground,

$$z = q \sin\left(\frac{2\pi x}{L}\right). \tag{46}$$

Note that the maximum and minimum amplitudes of the ground are $\pm q$ while L is its period. The coordinates of reflection points, required to calculate the multipath factor, are determined by the Eq. (14b). If the ground is flat, $h(x_R) = 0$ and then (14b) reduces to (4). Therefore, the horizontal positions of the observer x_O and source x_S affect the attenuation and phase only through their difference $x = x_O - x_S$ in the case of flat ground (the only parameter that influences the result is merely x and not x_O and x_S themselves), with the results represented in Figures 6 to 13. However, in the case of an undulated ground, represented in Figures 14 to 17, the positions of the source x_O and observer x_S relative to the undulations affect the attenuation and phase. In this case, as the ground is a periodic function, if the horizontal coordinates of observer and source are changed, while keeping the same distance x between them and their vertical coordinates z_S and z_O, the SPL and phase changes would be periodic with x_O (or with $x_S = x_O - x$).

Figures 14 to 16, similar to Figures 8 to 10 respectively, continue to show the SPL variations (left) and phase (right) shifts for a sound wave of one frequency $f = 1$ kHz. The ground is acoustically hard, $\mathcal{R} = 1$, because it corresponds to the worst case scenario of noise monitoring. The amplitude of the ground is always $q = 3$ m, but its period varies: $L = 20$ m (top plots), $L = 40$ m (middle plots) or $L = 60$ m (bottom plots). Figures 8 to 10 for flat ground correspond to $L = \infty$ and all these plots are very similar, consisting on several peaks and troughs and they have the same range values: approximately 6 to -30 decibels in SPL change and 90 to -90 degrees in phase shift. All these plots are derived from the same physical assumptions and indeed the plots for flat ground can be done by assuming that L is very large (ideally, tending to infinity).

Figures 8 and 14 show the dependence of the intensity (left) and phase (right) changes on the observer height, respectively, for flat and undulating grounds. As the height of the observer over ground increases, the amplitude and phase oscillations decrease for flat ground (Figure 8); the same happens to undulating ground. These peaks and troughs decrease in modulus with z_O because as the observer stays in a higher position, the ray path of reflected wave usually became longer (it is possible to consider another ground to became shorter but this it is not the case), decreasing therefore the ratio $r_1/(r_2 + r_3)$, and because of the proportional decaying of the acoustic amplitude with the propagation distance (due to the characteristic of a spherical wave), the reflected wave is losing its "strength". This is the same reasoning to explain the decreasing of peaks and troughs in modulus for the flat ground in Figure 8 and can be applied independently of the horizontal coordinate of observer and the characteristics of the ground, as one can conclude from the Figure 14. Note however that it is possible to consider another ground in such a way that, as the height of observer increases, the total ray distance of the reflected wave shortens because the shortening of the distance r_2 due to the new location of the reflection point is more considerable than the increment of the distance r_3, leading consequently to opposite conclusions. The undulation of the ground leads to two new features. In the middle plot, for $L = 40$ m, the solid line is invisible for $z_O < 3$ m (middle plots of Figure 14) because in that case the observer is under the line of sight and only when its height is higher than 3 m, the observer is able to receive acoustic waves. When the direct wave cannot reach the observer's position, the SPL and phase of the multipath factor are not plotted. The other feature occurs, for instance, when $L = 20$ m and $x_O = 60$ m, corresponding to the dotted lines of top plots in Figure 14. The signal interruptions that are visible in the top plots occur for the shortest undulation $L = 20$ m of the same height $q = 3$ m, that have a larger slope and can block the line of sight from the source to the observer, more frequent in the grazing directions. With the specific values of Figure 14, the SPL and phase values are always zero, independent of z_O, because there is no reflected wave that can reach the observer's position. These two new features are also visible in the subsequent figures.

Table 2: Parameters for Figures 14 and 15.

Line type	Position		
	Observer x_O [m]	Source x_S [m]	Difference $x_O - x_S$ [m]
Solid	10	0	10
Dashed	35	0	35
Dotted	60	0	60

Figures 9 and 15 show the dependence of intensity (left) and phase (right) oscillations on source height, respectively for flat and undulating grounds. In this figure, the observer is always 2 meters above the ground. Increasing the source height leads to a greater spacing of oscillations for flat (Figure 9) and undulating grounds (Figure 15). The reasons are the same for both types of ground. The parameter that explains the spacing of oscillations is the difference of ray paths, $r_2 + r_3 - r_1$, and if the ratio of that difference with z_s is lowering, the space between oscillations starts to increase;

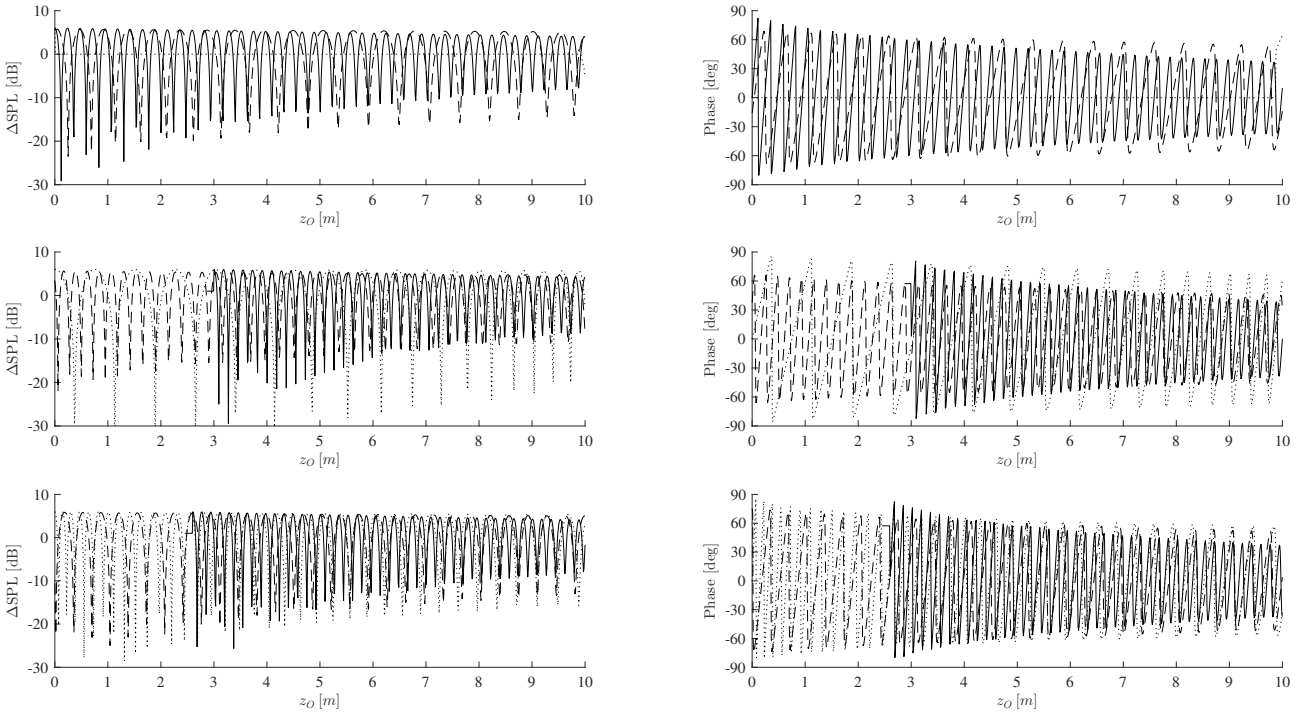

Figure 14: Sound attenuation and phase shift as functions of observer height z_O, for hard ground $\mathcal{R} = 1$ and undulating ground (46) with $q = 3$ m and for $L = 20$ m (top), $L = 40$ m (middle) and $L = 60$ m (bottom). The sound frequency is $f = 1$ kHz, the source is at a height $z_S = 30$ m and at a horizontal position $x_S = 0$ m, while the observer has different distances from the source, $x_O = \{10, 35, 60\}$ m for solid, dashed and dotted lines, as indicated in the Table 2.

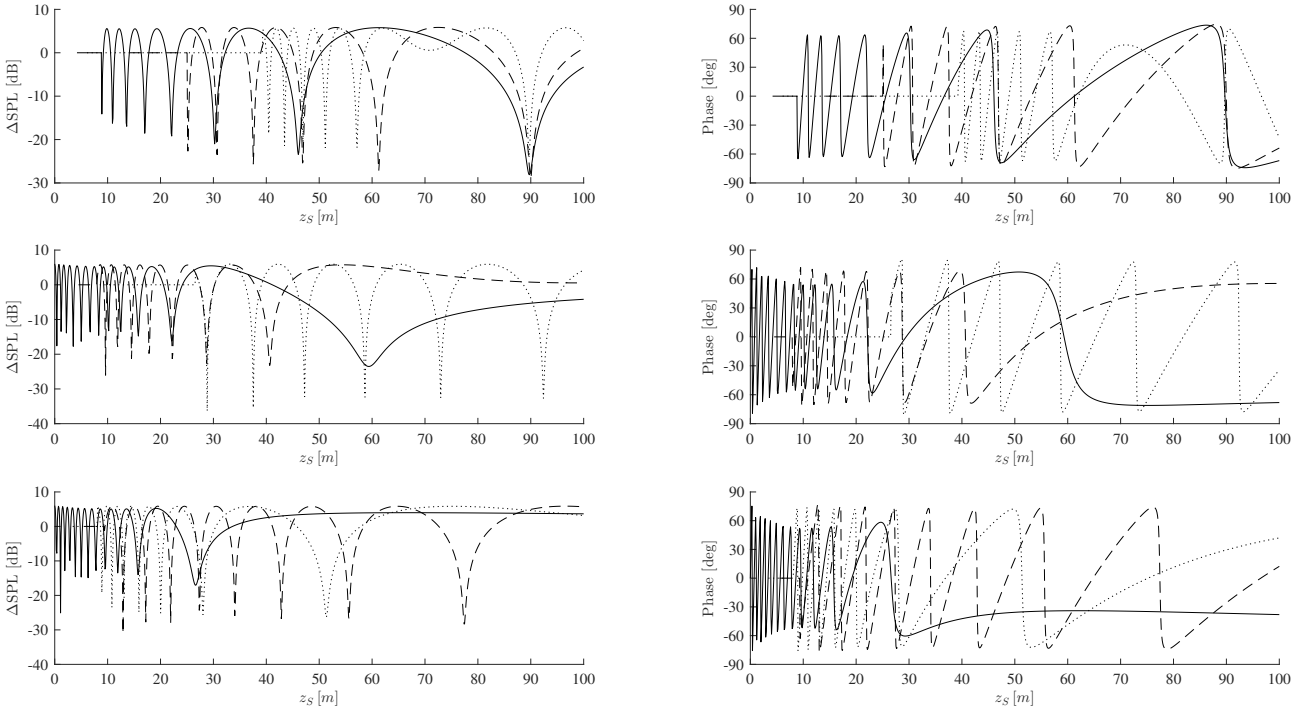

Figure 15: Sound attenuation and phase shift as functions of source height z_S, for hard ground $\mathcal{R} = 1$ and undulating ground (46) with $q = 3$ m and for $L = 20$ m (top), $L = 40$ m (middle) and $L = 60$ m (bottom). The sound frequency is $f = 1$ kHz, the source is at a horizontal position $x_S = 0$ m while the observer is always 2 meters above the ground, $z_O = 2$ m, but with different distances from the source, $x_O = \{10, 35, 60\}$ m for solid, dashed and dotted lines, as indicated in the Table 2.

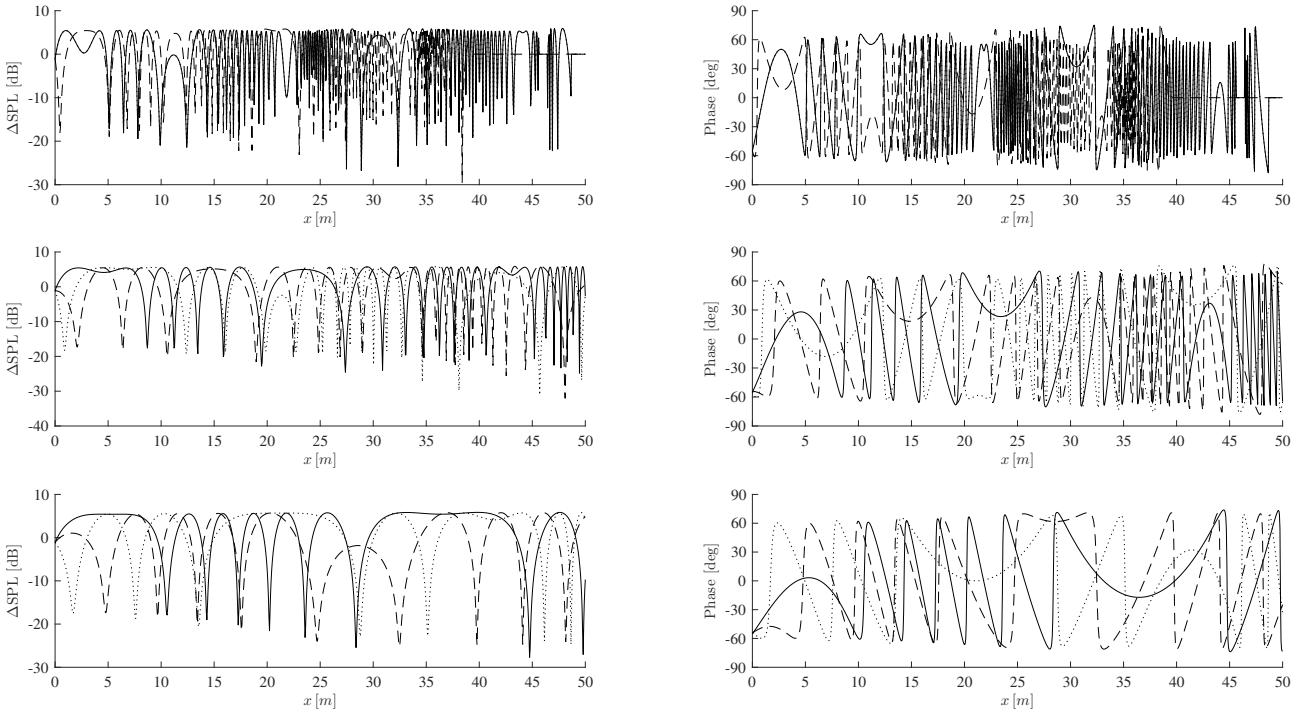

Figure 16: Sound attenuation and phase shift as a function of observer-source distance x, for hard ground $\mathcal{R} = 1$ and undulating ground (46) with $q = 3$ m and for $L = 20$ m (top), $L = 40$ m (middle) and $L = 60$ m (bottom). The sound frequency is $f = 1$ kHz, the source is at a height $z_S = 30$ m, and at the horizontal position $x_S = 0$ m while the observer is always 2 meters above the ground, $z_O = 2$ m, but with its distance from the source varying continuously since $x_O = x + x_S$.

on the other hand, if that ratio is increasing, the space starts to narrow. The same conclusion can be reached by observing at the cosine and sine arguments in the equations (16b) and (17b). The variation with z_S influences more the parameter $r_2 + r_3 - r_1$ than the parameter $r_1/(r_2 + r_3)$,which is approximately constant with z_S and therefore the amplitude of extreme points remains constant. Shorter undulations do not affect much the spacing of oscillations, but introduce a blocking of the line-of-sight and signal cut-off visible for steeper undulations, $L = 20$ m (top) or even $L = 40$ m (middle), and absent for shallower undulations, $L = 60$ m (bottom) or for the extreme case of flat ground (Figure 9). Since the height of undulations is fixed ($q = 3$ m) in Figures 14 and 15, the shorter undulations have steeper slope q/L and lead to the blocking of the line-of-sight from the source to the observer in the grazing directions (not forgetting that the block of signals is also very influenced by the position of observer and source).

Figures 10 and 16 concern the effect of horizontal distance between source and observer respectively for flat and undulating grounds. In this figure, the observer is again 2 meters above the ground, but the source positions is different for each type of line: $x_S = 0$ m for solid, $x_S = 10$ m for dashed and $x_S = 20$ m for dotted line. The intensity (left) and phase (right) oscillations are affected both in magnitude and spacing (although the effect is more noticeable in the spacing), not only for flat (Figure 10) but also for undulating grounds (Figure 16). The signal interruptions again occur for shorter or steeper undulations and grazing directions associated with larger distances from the source to the observer (for instance, the dashed line, with $x_S = 10$ m, of top plots with $L = 20$ m). Note that the dotted line of top plots follows exactly the solid one because both lines represent the same situation since the ground is periodic with $L = 20$ m.

Whereas Figures 10 to 16 keep the height of undulations and vary their length, the reverse applies in the final Figure 17. The sound intensity is constant for flat ground $q = 0$ m, and depends on the length L of undulations for non-flat ground $q = 1, 2, 3, 4$ m. In all the plots of the Figure 17, the source is at the height $z_S = 30$ m while the observer is 2 meters above the ground. The horizontal coordinates of observer and source are indicated in the Table 3. They are in the same vertical plane as crests or troughs of the different ground profiles. That remark is also indicated in the Table 3. The sound level goes always through several minima and maxima, corresponding respectively to destructive and constructive interferences, that occur for smaller and more numerous values of the length of undulations L if the horizontal distance between the observer and source x

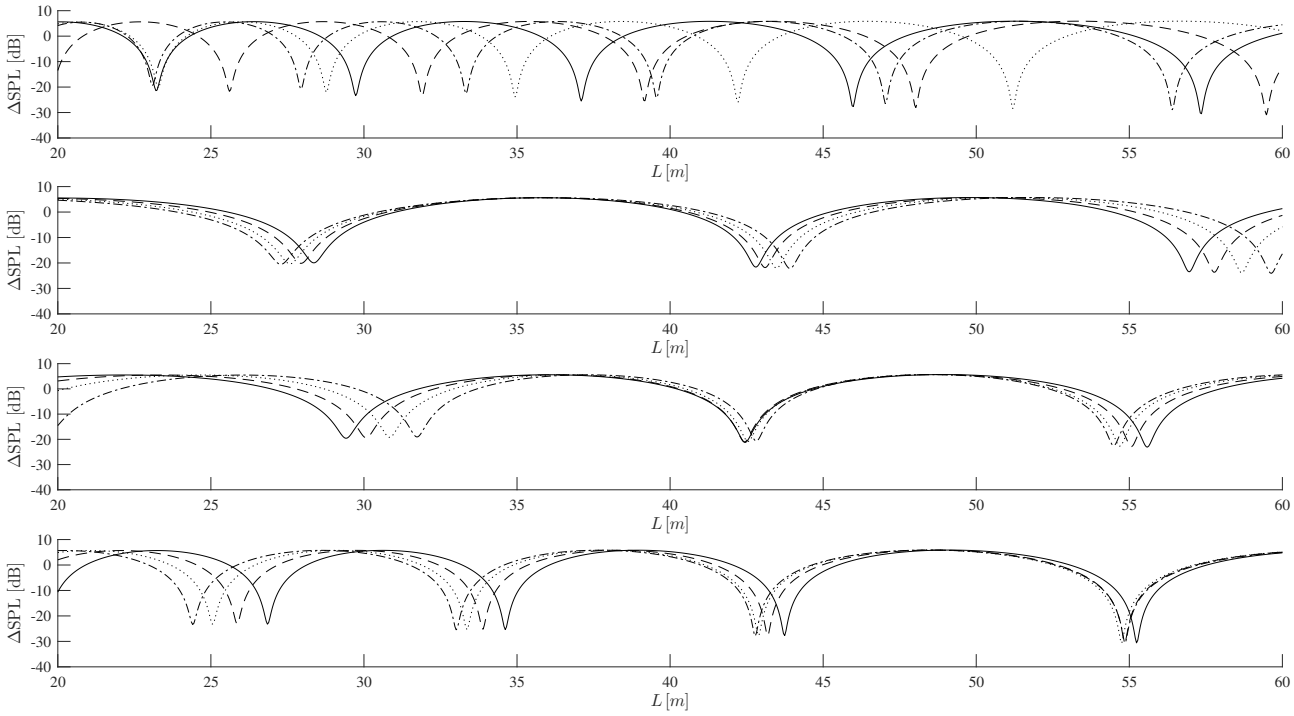

Figure 17: Sound attenuation as a function of L for hard $\mathcal{R} = 1$ and undulating ground with $q = 0$ (solid line), $q = 1$ (dashes), $q = 2$ (dots), or $q = 3$ (dot-dash). The sound frequency is $f = 1$ kHz, the observer is at a height $z_O = 5$ m, the source is at a height $z_S = 30$ m, and at a horizontal distance between source and observer is $x = 50$ m.

increases. There is no great difference in the results when the amplitude of the ground q changes. The effect on the multipath factor is more noticeable when the length of undulations is modified. However, keeping the ground undulating like a sine function does not alter the range of SPL changes: approximately -30 to 6 decibels.

The range of SPL aforementioned is valid for all the plots of Figures 14 to 17. This is a consequence that is very rare to have more than one reflected wave that can reach the observer's position. Almost in all situations of the undulating ground, there is only one solution of the Eq. (14b), indicating that there is only one reflection point and consequently two waves reach the observer: one direct from the source plus one reflected from the ground. For the ground profile (46), the model II can be analysed a priori by the results of the model I that studies the situation of flat ground where the same number of waves reaches the observer. However, this model II does not take into account multiple reflections on the ground and that explains why in almost every cases there is only one reflected wave. If one considers waves that can imping on the ground several times and then reach the observer, hence there will be more reflected waves with the main difference being the maximum theoretical value of the SPL changes: instead of 6.02 decibels, with 2 reflected waves it can be at maximum 9.53 decibels, or with 3 reflected waves the maximum value can be 12.04 decibels. The case of multiple reflections before reaching the observer should occur only for very particular directions of propagation.

Table 3: Horizontal coordinates of the observer and source for the Figure 17.

Sub-figure	Horizontal coordinate		
	Observer x_O [m]	Source x_S [m]	Difference $x_O - x_S$ [m]
First	$5L/4$ (crest)	$L/4$ (crest)	L
Second	$3L/4$ (trough)	$L/4$ (crest)	$L/2$
Third	$5L/4$ (crest)	$3L/4$ (trough)	$L/2$
Fourth	$7L/4$ (trough)	$3L/4$ (trough)	L

7 Conclusion

Aircraft noise [1, 2] contours at airports [23, 24] are currently predicted using the model of a point source of sound at the aircraft with effect of flat ground represented by an image source [12–20, 25–28]. The real environment around airports may involve non-flat ground, such as buildings that

act as corner reflectors [21] or uneven and mountainous terrain that can cause reflections from several points. In the case of flat ground, an alternative to the (I) method of images is the (II) method of reflected waves. To the direct wave from the real sound source to the observer, the method I adds a virtual sound wave from the image source that is replaced in the method II by a wave reflected from the ground. In both methods I and II, the acoustic boundary condition on the ground must be met. In the case of the method II of reflection, this leads to a reflection coefficient that is complex, including both amplitude and phase changes. In the case of the method I, the amplitude and phase are specified by the position and strength of the image source.

Both methods of (I) images and (II) reflections apply to building effects on sound, like a corner reflector. Using the method I of images, there are three images [22]: on the ground, on the wall and in the apex. Using the method II of reflected waves [21], there are also three reflected waves: on the ground, on the wall and on both. The applicability of the two methods differs in the case of rough ground: (i) the method of images does not extend readily to rough ground, as it is necessary to find the location and strength of possibly several image sources; (ii) the method of reflections extends to rough ground by identifying all reflection points, applying the corresponding reflection coefficients and adding all waves in line-of-sight of the observer. After the method II of reflection points is applied to rough ground, it would be possible to identify a set of equivalent image sources for the method I of images, but this would be redundant. Most of the acoustic measurements and experiments compare with theories of sound reflection from flat ground, and do not record the terrain profile. The comparison of the present theory of sound reflection by rough ground with experiments would require both the acoustic signal and terrain profile.

The problem of ground effect and atmospheric attenuation on aircraft noise can be addressed by a sequence of three progressively more sophisticated models. The models evolve from (i) a single reflection from flat ground, to (ii) multiple reflection from rough ground; atmospheric absorption can be included with (i) uniform or (ii) non-uniform attenuation. The ground may be (i) rigid or have (ii) a uniform impedance or (iii) a reflection coefficient with specified amplitude and phase. Some of these many possibilities were illustrated, namely the influence of source and observer heights, relative horizontal distance and frequency on sound intensity and phase, for: (i) flat ground either rigid or with complex reflection coefficients; (ii) non-flat ground with sinusoidal shape allowing choice of two parameters, namely height and length of undulations. The rough ground models allow for arbitrary terrain profiles, and are by no means restricted to the simple sinusoidal shape used.

Acknowledgement: This work was supported by the project COSMA of the EU Aeronautics Program. This work was also supported by the Fundação para a Ciência e Tecnologia (FCT), Portugal, through Institute of Mechanical Engineering (IDMEC), under the Associated Laboratory for Energy, Transports and Aeronautics (LAETA), whose grant numbers are UIDB/50022/2020 and SFRH/BD/143828/2019.

Author contributions: All authors have accepted responsibility for the entire content of this manuscript and approved its submission.

Conflict of interest: The authors state no conflict of interest.

References

[1] Smith MJ. Aircraft Noise. Cambridge: Cambridge University Press; 1989. https://doi.org/10.1017/CBO9780511584527
[2] Zaporozhets O, Tokarev V, Attenborough K. Aircraft Noise: Assessment, prediction and control. 1st ed. London: CRC Press; 2011. https://doi.org/10.1201/b12545.
[3] Delany ME. Sound propagation in the atmosphere: a historical review. Acoustica. 1977;38(4):201-223.
[4] Piercy JE, Embleton TF, Sutherland LC. Review of noise propagation in the atmosphere. J Acoust Soc Am. 1977 Jun;61(6):1403–18.
[5] Brown EH, Hall FF Jr. Advances in atmospheric acoustics. Rev Geophys. 1978;16(1):47–110.
[6] L'Espérance A, Herzog P, Daigle GA, Nicolas JR. Heuristic Model for Outdoor Sound Propagation Based on an Extension of the Geometrical Ray Theory in the Cae of a Linear Sound Speed Profile. Appl Acoust. 1992;37(2):111–39.
[7] Bass HE, Sutherland LC, Zuckerwar AJ, Blackstock DT, Hester DM. Atmospheric absorption of sound: further developments. J Acoust Soc Am. 1995;97(1):680–3.
[8] Attenborough K, Taherzadeh S, Bass HE, Di X, Raspet R, Becker GR, et al. Benchmark cases for outdoor sound propagation models. J Acoust Soc Am. 1995;97(1):173–91.
[9] Sutherland LC, Daigle GA. Atmospheric sound propagation. In: Crocker MJ, editor. Handbook of Acoustics. New York (NY): Wiley; 1998. p. 305–29.
[10] Campos LM. The spectral broadening of sound by turbulent shear layers. Part 1. The transmission of sound through turbulent shear layers. J Fluid Mech. 1978;89(4):723–49.
[11] Campos LM, Cunha FS. On the power spectra of sound transmitted through turbulence. Int J Aeroacoust. 2012;11(3-4):475–520.
[12] Ingard KU. On the Reflection of a Spherical Sound Wave from an Infinite Plane. J Acoust Soc Am. 1951;23(3):329–35.
[13] Li KM. A high-frequency approximation of sound propagation in a stratified moving atmosphere above a porous ground surface.

J Acoust Soc Am. 1994;95(4):1840–52.
[14] Campos LM, Serrão PG. On the effect of atmospheric temperature gradients and ground impedance on sound. Int J Aeroacoust. 2014;13(5-6):427–48.
[15] Sommerfeld A. Über die Ausbreitung der Wellen in der drahtlosen Telegraphie. Ann Phys. 1909;333(4):665–736.
[16] Rudnick I. The Propagation of an Acoustic Wave along a Boundary. J Acoust Soc Am. 1947;19(2):348–56.
[17] Raspet R, Lee SW, Kuester E, Chang DC, Richards WF, Gilbert R, et al. A fast-field program for sound propagation in a layered atmosphere above an impedance ground. J Acoust Soc Am. 1985;77(2):345–52.
[18] Landau LD, Lifshitz EM. Fluid mechanics. 2nd ed. Oxford: Pergamon Press; 1987.
[19] Raspet R, Baird G, Wu W. Normal mode solution for low-frequency sound propagation in a downward refracting atmosphere above a complex impedance plane. J Acoust Soc Am. 1992 Mar;91(3):1341–52.
[20] Taraldsen G. A note on reflection of spherical waves. J Acoust Soc Am. 2005 Jun;117(6):3389–92.
[21] Campos LM, Silva MJ, Fonseca AR. On the multipath effects due to wall reflections for wave reception in a corner. Noise Mapp. 2021;8(1):41–64.
[22] Campos LM. Complex Analysis with Applications to Flows and Fields. 1st ed. Boca Raton (FL): CRC Press; 2011.
[23] Pao SP, Wenzel AR, Oncley PB. Prediction of Ground Effects on Aircraft Noise. NASA Technical Paper 1104; 1978
[24] ICAO Doc 9911: Recommended Method for Computing Noise Contours Around Airports. 2nd ed. Montréal, 2018
[25] Wenzel AR. Propagation of waves along an impedance boundary. J Acoust Soc Am. 1974;55(5):956–63.
[26] Delany ME, Bazley EN. Monopole radiation in the presence of an absorbing plane. J Sound Vibrat. 1970;13(3):269–79.
[27] Delany ME, Bazley EN. A note on the effect of ground absorption in the measurement of aircraft noise. J Sound Vibrat. 1971;16(3):315–22.
[28] Chien CF, Soroka WW. Sound propagation along an impedance plane. J Sound Vibrat. 1975;43(1):9–20.